Taurine supplementation activates growth suppression mechanisms in ovarian cancer.

Daniel Centeno[1], Sadaf Farsinejad[1], Elena Kochetkova[2], Tatiana Volpari[3], Agnieszka Klupczynska – Gabryszak [4], Douglas Kung[1], Teagan Polotaye[1], Emily Hyde[1], Michael Greenberg[1], Tonja Pavlovic[1], Sarah Alshehri[1], William Sullivan[3], Szymon Plewa[4], Helin Vakifahmetoglu-Norberg[2], Frederick J Monsma, Jr[3]. , Patricia A. J. Muller[7], Jan Matysiak[4], Mikolaj Zaborowski[5], Analisa Difeo[6], Laura A. Martin[3*], Erik Norberg[2*], and Marcin Iwanicki[1*].

1. Department of Chemistry and Chemical Biology, Stevens Institute of Technology, Hoboken, NJ USA
2. Department of Physiology and Pharmacology, Karolinska Institute, Stockholm, Sweden
3. The New York Stem Cell Foundation Research Institute, New York, NY USA
4. Department of Inorganic and Analytical Chemistry, Poznań University of Medical Sciences, Poznań, Poland
5. Department of Gynecology, Obstetrics and Gynecologic Oncology, Poznań University of Medical Sciences, Poznań, Poland
6. Departments of Obstetrics and Gynecology and Pathology, University of Michigan, Ann Arbor, MI USA
7. Department of Biosciences, Durham University, Durham, United Kingdom

* correspondence: miwanick@stevens.edu (lead), erik.norberg@ki.se, landresmartin@NYSCF.org

ABSTRACT

Loss of treatment-induced ovarian carcinoma (OC) growth suppression poses a major clinical challenge because it leads to disease recurrence. Therefore, there is a continuous need for approaches that can maintain OC suppression after treatment. We have profiled ascites as OC tumor microenvironments (TMs) to search for potential soluble components that would exert growth suppression on OC cell cultures. Our investigations revealed that low levels of taurine, a non-proteogenic sulfonic amino acid, were present within OC ascites. Taurine supplementation, beyond levels found in ascites, induced growth suppression without causing cytotoxicity in multiple OC cell cultures, including chemotherapy-resistant cell clones and multiple patient-derived organoids. Suppression of proliferation by taurine was associated with increased mutant or wild-type p53 proteins binding to DNA and induction of p21 and TIGAR expression. Taurine suppressed the cell-cycle progression, glycolysis, and mitochondria respiration. Expression of

p21 or TIGAR in OC cells, in part, mimicked taurine-induced inhibition of cell proliferation. Our studies support the potential therapeutic value of taurine supplementation in OC.

INTRODUCTION

Ovarian Carcinoma (OC) often recurs after aggressive and exhaustive rounds of cytotoxic and targeted therapies[1]. The recurrence is due to the ability of tumor cells to overcome treatment-induced tumor suppression, and re-initiate proliferation[2] which contributes to disease progression and poor patient outcomes[3]. Therefore, the development of strategies that maintain suppression of cancer cell proliferation represents a continuous need.

The tumor protein p53 (p53) is a major tumor suppressor molecule that is mutated in a significant proportion of OCs[4,5]. One of the tumor suppressive functions of p53 is to inhibit proliferation through the activation of cyclin-dependent kinase inhibitor 1A (p21) CDKN1[6,7]. Low levels of nuclear p21 protein in OC-expressing p53 mutant proteins correlate with tumor cell proliferation and reduced progression-free intervals[8-11]. In addition to the regulation of the cell cycle[12], loss of p53 activity is frequently associated with increased glycolysis[13] and metabolic dysfunction in cancer[14]. Considering these data, multiple synthetic chemistry-based approaches have been used to restore mutant p53 activation of p21[15-18]; however, these approaches, in addition to activation of p21, can induce toxicities that might potentially pose a clinical challenge.

Interestingly, despite a high frequency (up to 30%) of *TP53* mutations in the cell-of origin of OC, the fallopian tube non-ciliated epithelial (FNE) cells[19-21], the lifetime risk of developing OC is less than 1.5% [22]. These observations pose an important question of whether components of tissue microenvironments (TMs) can support tumor suppressive functions of various p53 proteins.

Factors within TMs could modulate cancer growth through engagement of molecules expressed on the surface of transformed cells[23]. Therefore, knowing the cell surface proteome of FNE cells expressing mutant p53 can potentially lead to the identification of TM components, that through engagement of cell surface proteins, activate tumor suppressive signals.

We have profiled the cell surface proteome of FNE cells and identified that mutant p53 (m-p53) promotes expression of a taurine transporter, SLC6A6. Taurine is a natural product of body metabolism[24], it can be synthesized from intracellular cysteine pools[25], and its tissue concentrations decreases with aging[26]. Taurine functions as an osmolyte to regulate cell size and volume[27-32]. In addition to the regulation of cell and tissue homeostasis, taurine supplementation has been found to improve (1) cognitive functions[33], (2) glucose metabolism[34], (3) bone homeostasis[35], (4) motor functions[36] , and (5) activate anti-aging mechanisms in worm and mice[26]. Taurine stimulates signal transduction downstream of neuronal cell surface receptors for glycine GlyR[37], glutamate (N-Methyl D-Aspartate Receptor)[38] and, in non-neuronal cells, G-protein coupled 87 (GPR87)[39] receptor. Taurine, in most cells, can be transported into cells via a sodium/chloride-dependent symporter, SLC6A6[40]. A few recent reports provided evidence that taurine supplementation suppresses the growth of colon, cervical and endometrioid cancer cells[41-43]; however, the mechanisms of tumor suppression by taurine are not well understood.

Using a combination of transcriptomic, cell biologic, and biochemical approaches, we provide evidence that supplementation of various monolayer, spheroid, and organoid OC cell cultures with taurine activates p53-dependent and independent tumor suppression pathways leading to inhibition of OC cell growth without causing cytotoxicity. Taurine-mediated growth suppression was associated with a ~12-20-fold increase in intracellular taurine levels, cell volume increase, p53 biding to DNA, and activation of p21 promoter in OC cells carrying mutant or wild-type p53 proteins. Moreover, in OC cells lacking p53 protein expression (due to nonsense mutation), taurine did not activate p21 but did induce expression of the phosphatase TIGAR, a negative regulator of glycolysis. Taurine induced increase in TIGAR expression correlated with suppression of glycolysis and mitochondrial oxidative phosphorylation. Ectopic expression of p21 or TIGAR in OC cell lines partially mimicked taurine's tumor suppressive activities. Our studies indicate that elevation of taurine levels within TMs could potentially suppress OC proliferation through the activation of p21 and/or TIGAR signal transduction pathways.

RESULTS

Proteomic screen identifies taurine transporter enrichment in suspended fallopian tube non-ciliated epithelial (FNE) cells expressing mutant p53^{R175H}.

We have previously reported that mutant p53 expression in FNE cells supports OC-transformed phenotypes including ECM-induced outgrowths[44], anchorage-independent survival, and mesothelial intercalation[45]. To further investigate the changes associated with mutant p53 expression in FNE cells, we have compared the cell surface proteomes of control FNE cells expressing empty plasmid and FNE cells overexpressing plasmid containing mutant p53^{R175H} (FNE-m-p53). Based on the Weekes *et al.* methodology of cell surface protein purification[46] we performed three independent tandem-mass-tag-based mass spectrometry[47] experiments and found 110 differentially expressed proteins (Fig. 1A). Only proteins that appeared in all three experiments were included in the analysis. Our analysis revealed that one of the significantly enriched cell surface proteins in FNE-m-p53 was SLC6A6 (Fig. 1B), a taurine transporter. The literature supports transcriptional suppression of SLC6A6 by wild-type (WT) p53[48]; thus, we wanted to verify whether the expression of mutant p53 increases SLC6A6 levels in FNE cells. Due to the lack of suitable SLC6A6 antibody, we used quantitative polymerase chain reaction (qPCR) to validate SLC6A6 primers in HEK293 cells overexpressing a plasmid containing the SLC6A6 gene (S. Fig. 1A) and, based on the validation experiment used appropriate primers to measure transcripts levels among syngeneic FNE cell lines that express WT p53 or mutant p53^{R175H} (m-p53^{R175H}). We found that ectopic expression of m-p53^{R175H} in FNE cells significantly increased SLC6A6 mRNA levels (Fig. 1C). These results validated our proteomic data and indicated the possibility that the taurine transporter is expressed in OC cells. So, we profiled SLC6A6 mRNA expression levels in seven additional OC cell lines and observed differential

expression of SLC6A6 among these cell lines, with the highest expression in cells carrying mutant p53^{R175H} (Fig.1D). Our data are consistent with the idea that SLC6A6 is expressed in OC cells.

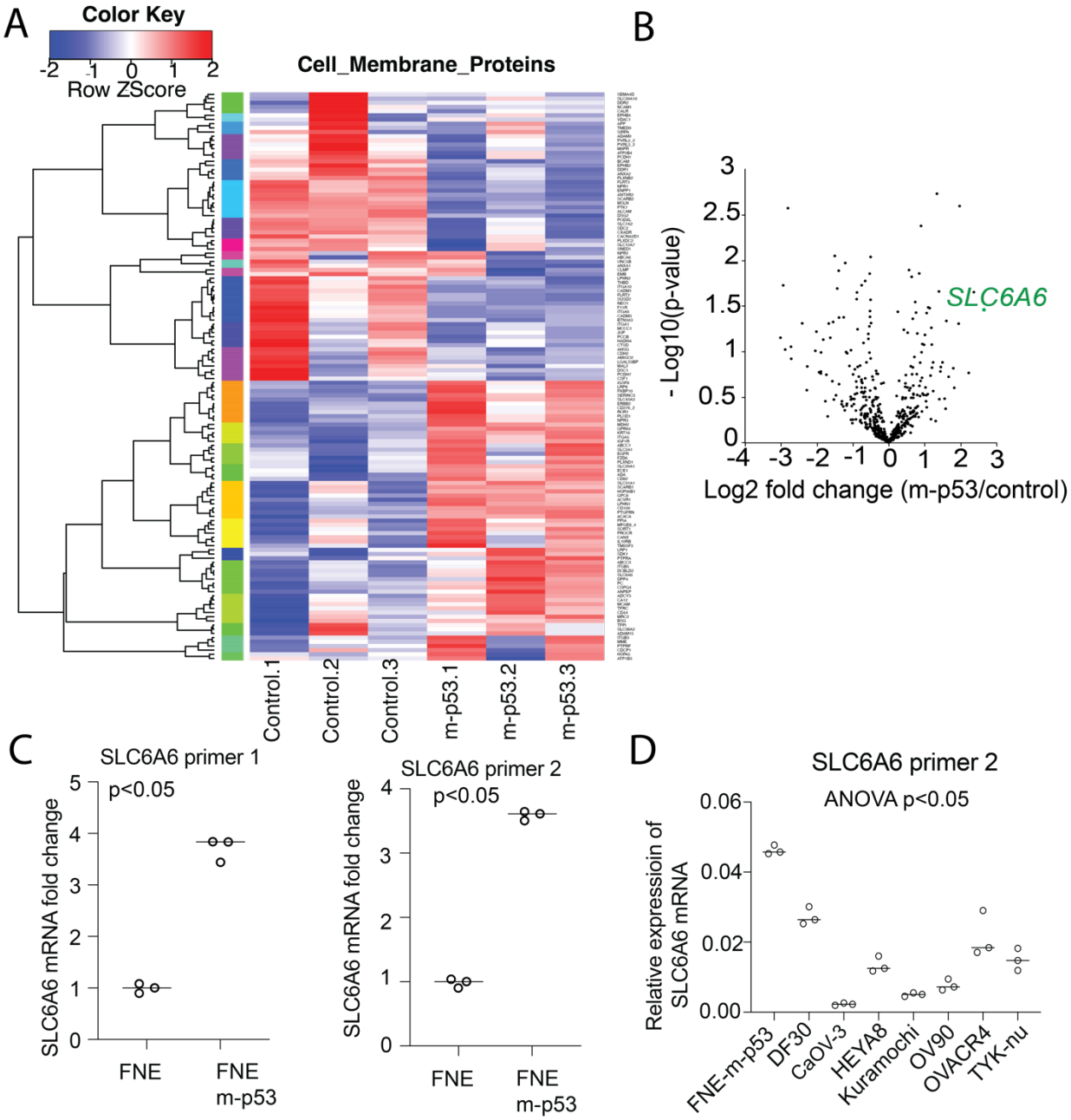

Figure 1. *(A)* Heat map representation of 110 cell surface protein expressions significantly changed between FNE cells carrying empty plasmid (control) or plasmid containing mutant p53^{R175H} (m-p53). Each column (control.n, m-p53.n) represents one replicate. *(B)* Volcano plot of all differentially expressed proteins. A labeled green dot represents the SLC6A6 protein. *(C-D)* SLC6A6 mRNA levels in syngeneic FNE cells and various OC cell lines. Each dot represents one replicate. An unpaired, two-sided t-test (in C) or ANOVA (in D) was used to determine statistical differences between the means.

Taurine is a component of OC tissue microenvironments (TMs) and taurine supplementation suppresses OC cell proliferation.

The expression of taurine transporter in various OC cell lines suggested the possibility that taurine, a constituent of the human body, is present within OC TMs. To explore this possibility, we used mass spectrometry to profile 16 ascites samples isolated from patients representing primary and recurrent diseases. We found that taurine concentration within ascites varied from 30-125 μM (Fig. 2A). Taurine is an osmolyte implicated in the regulation of cell volume[28-32]. Depletion of taurine also decreases cell size[49] and a recent report suggested that cell area and cell volume increase was associated with the suppression of cell proliferation[50]. Based on this information, we wondered whether taurine supplementation, at the levels found in ascites, increases cell area, cell volume and modulates cell proliferation. We treated a DF30 cell line expressing green fluorescent protein (GFP) with 100 μM of taurine for 72 hours. Following taurine treatment, we used fluorescent microscopy to image single adherent or suspended DF30 cells. Based on microscopy recordings we measured the cell area/volume and cell proliferation. We found that 100 μM taurine supplementation did not affect cell area, cell volume, or cell proliferation as determined by live-cell microscopy recordings of cell number changes over 72 hours (S. Fig 1B). Our data indicate that supplementation of DF30 cell cultures, with taurine concentrations similar to those detected in patient ascites does not suppress OC cell proliferation. Because 80% of serum taurine levels decrease by the fifth decade of life[26], we explored a possibility that increasing taurine beyond the levels found in ascites, might increase cell area, cell volume, and suppress OC cell proliferation. To explore this possibility, we first determined the concentration of taurine that evokes an increase in cell area. We found that 160 mM taurine supplementation increased the average cell area of adherent DF30 cells from 2500 μm^2 to 5000 μm^2 (Fig. 2B,

MOVIE 1). We also observed a ~30% increase in suspended DF30 cell volume in response to 160-mM taurine supplementation (Fig. 2C).

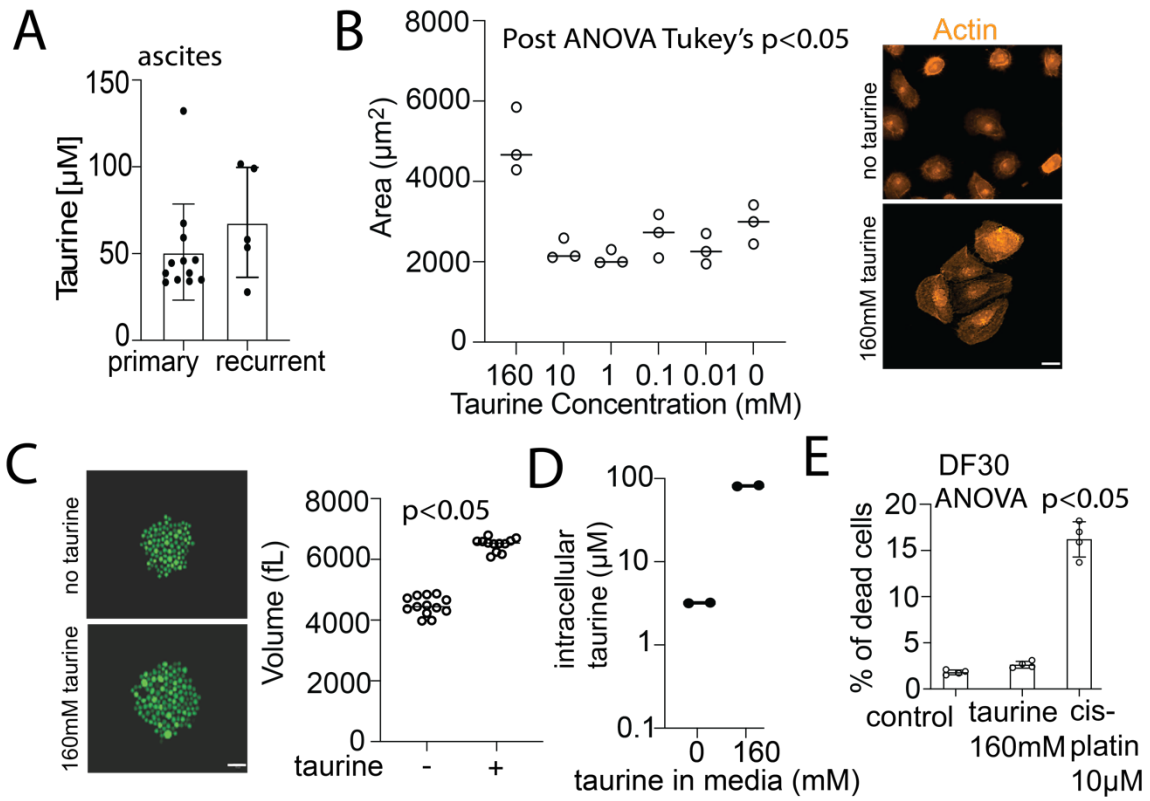

Figure 2. *(A)* Taurine concentration in primary and recurrent ascites. Each dot represents ascitic fluid from one OC patient. *(B)* Quantification of cell adhesion area in DF30 cell monolayer cultures supplemented with various amounts of taurine. Each dot represents the mean area of one imaging replicate containing at least 300 cells. Fluorescent images of actin in DF30 cell cultures supplemented with media, or media containing 160 mM of taurine. Scale bar is 50 μm. Ordinary one-way ANOVA followed by Tukey's multiple comparison tests were performed with a p-value representing the difference between 0 mM and 160 mM taurine groups. *(C)* Fluorescent images of GFP expression in suspended DF30 cells cultured in the absence or the presence of 160 mM of taurine. Scale bar is 50 μm. The graph represents the quantification of suspended DF30 cell volume changes in response to taurine supplementation. Each dot represents the mean volume calculated from 100 cells. An unpaired two-sided t-test was used to determine the difference between the means. *(D)* The graph represents a mass spectrometry-based measurement of intracellular taurine in DF30 cell monolayers supplemented with media, or media containing 160 mM taurine. Each dot refers to one replicate. *(E)* Flow cytometry-based quantification of cell death based on propidium iodide (PI) incorporation by DF30 cells cultured under indicated conditions. Each dot represents the mean PI fluorescence of one experimental replicate. Ordinary one-way ANOVA was used to determine differences between the means.

Taurine-dependent increase in cell area and cell volume was associated with nearly 20-fold taurine influx (Fig. 2D), as measured by mass-spectrometry [51]. These changes in intracellular taurine concentration had no effect on cell viability (Fig. 2E), indicating that taurine supplementation does not cause cytotoxicity. shRNA-mediated attenuation of SLC6A6 in DF30 cells (S. Fig. 1C) moderately decreased taurine influx (S. Fig. 1D) indicating that in OC cells SLC6A6, at least in part, supports taurine import into the cytoplasm. Our data are consistent with the idea that taurine supplementation of OC cell cultures results in SLC6A6-dependent taurine influx that is associated with an increase of cell area and volume without causing cell cytotoxicity. Next, we wondered whether taurine supplementation could suppress OC cell proliferation. Our initial live-cell phase-contrast microscopy imaging revealed less frequent cell divisions in DF30 cells cultured in the presence of taurine (MOVIE 1 and Fig. 3A-B), indicating a possibility that taurine suppresses cell proliferation. As predicted, taurine supplementation suppressed DF30 and FNE-m-p53 cell proliferation (Fig. 3B). Image analysis of DF30 cell death as measured by propidium iodide (PI) incorporation into suspended structures confirmed that taurine does not cause cell death (S. Fig 1E). Motivated by these results, we wanted to extend taurine supplementation studies to multiple OC cell lines including chemotherapy resistance cell clones. Thus, we examined nine additional OC cell lines (Kuramochi, OV90, OVCAR4, TYK-nu, Hey-A8) including four syngeneic cell lines representing parental and chemotherapy-resistant cell clones [52], OV81, OV81-CP40 and OV231, OV231-CP30, cultured as adherent monolayers. Our examination found that taurine supplementation suppressed proliferation in all tested cell lines (Fig. 3C). In addition, we used suspended basement membrane (BM) reconstituted organotypic cultures of FNE-m-p53, OV90, Hey-A8, OV81-CP40 and OV231-CP30, to demonstrated that taurine significantly inhibited organotypic structure expansion (Fig. 3D-H). Taken together, our data suggest that taurine supplementation suppresses OC cell line proliferation without causing cytotoxicity.

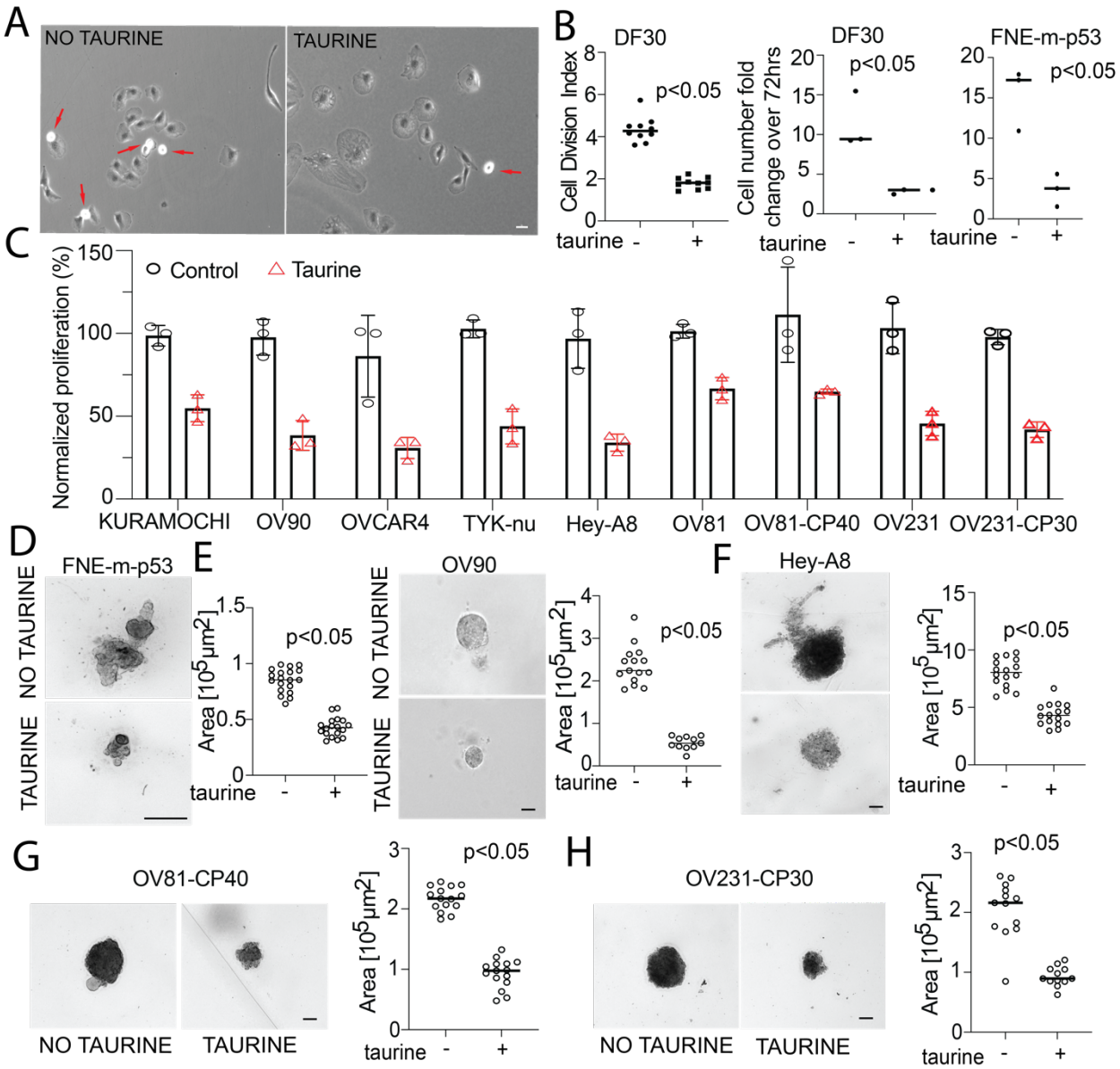

Figure 3. *(A)* Phase contrast images of DF30 cell monolayers cultured in the absence or presence of 160 mM taurine. Red arrows point to mitotic cells. Scale bar is 50 μm. *(B)* Quantification of cell division (based on time lapse recordings), and cell proliferation in DF30 and FNE-m-p53 cells supplemented with media or media containing 160 mM taurine. Each dot represents the mean of cell division events within one ROI containing 24-125 cells. In proliferation experiments each dot corresponds to one replicate counting. *(C)* Quantification of cell proliferation, based on automatic counting, of cell monolayers, supplemented with growth media or growth media containing 160 mM taurine. Each dot represents one replicate counting. *(D-H)* Phase contrast images and quantification of organotypic structure area under normal growth or taurine-supplemented reconstituted basement membrane conditions. Each dot represents one organotypic structure. An unpaired, and two-sided t-test was used to determine the difference between the means. Scale bars are 50 μm.

Taurine supplementation inhibits growth of OC patient-derived organoids.

Utilization of organoid cultures in cancer research can support experiments that interrogate cancer biology in the context of relevant TMs and carcinoma cell organization[53]. Therefore, we wanted to know whether taurine supplementation suppresses growth of patient-derived OC organoids (PDO). We used three organoid cultures, representing mucinous (PDO1) and high-grade serous (PDO9, PDO10) OC. PDO9 has been established from tissues previously exposed to neo-adjuvant chemotherapy, while both PDO1 and PDO10 represent chemotherapy naïve tumors. PDO cultures were dissociated into single cells and seeded embedded in basement membrane extract (BME) at 200 cells/μl for expansion up to nine days in the control media or media containing taurine. To follow PDO growth we used a combination of bright-field imaging, cell count and automated analysis of PDO area. Consistent with the cell line data (Fig. 3), we observed that taurine significantly decreased growth (Fig. 4A-B) and the surface area of PDOs (Fig. 4A-B), indicating that taurine suppresses PDO growth. CellTiter®-Glo 3D assays revealed that taurine decreased the ATP levels, indicating a possible suppression of cell metabolisms in PDOs (Fig. 4C). These results are consistent with the idea that taurine activates growth suppression mechanisms in OC.

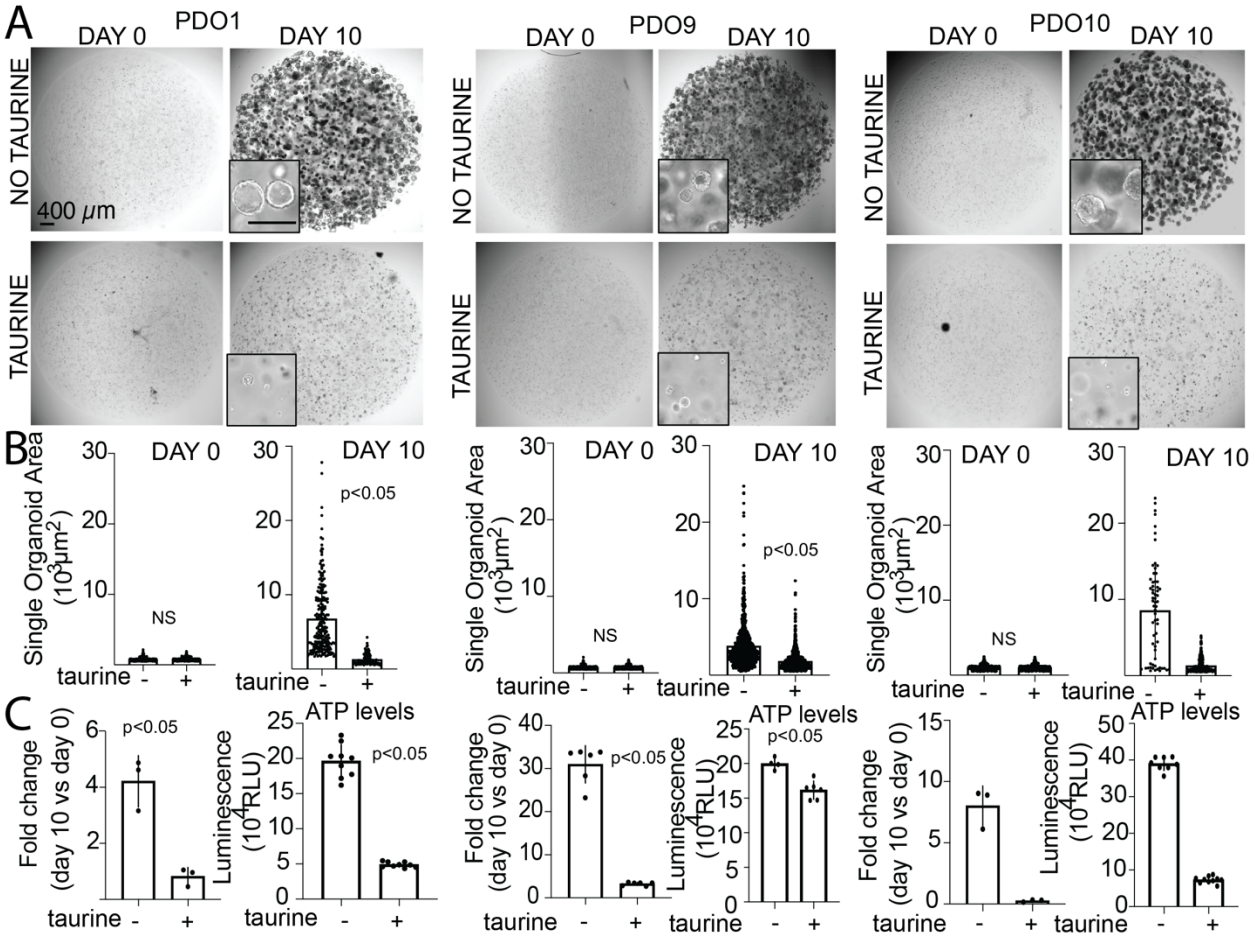

Figure 4. *(A)* Low and high (inset) magnification brightfield images of entire wells representing three PDO cultures at Day 0 and Day 10. Inset scale bar is 200 µm. (B) Quantification of single organoid area at day 0 and day 10, 100-700 organoids were quantified per group, each dot represents one organoid. *(C)* Left panels: Quantification of culture growth, each dot represents one well. Right panels: End point measurement of ATP levels using CellTiter-Glo® assay, each dot represents luminescence value recorded from one well. Unpaired, non-parametric two-tailed t-tests with Welch's correction were used to determine the difference between groups.

Taurine activates p53 pathway in OC cells expressing mutant or wild-type p53 protein.

To gain mechanistic insights associated with taurine-mediated suppression of proliferation we performed transcriptomic analysis of DF30 cell cultures supplemented with taurine. Our experiment revealed taurine-induced enrichment of genes associated with the activation of the *TP53* regulatory pathway, particularly p53-dependent negative regulation of cell proliferation (Fig. 5A) including activation of the cyclin-dependent kinase inhibitor 1A (CDKN1A; also known as p21)

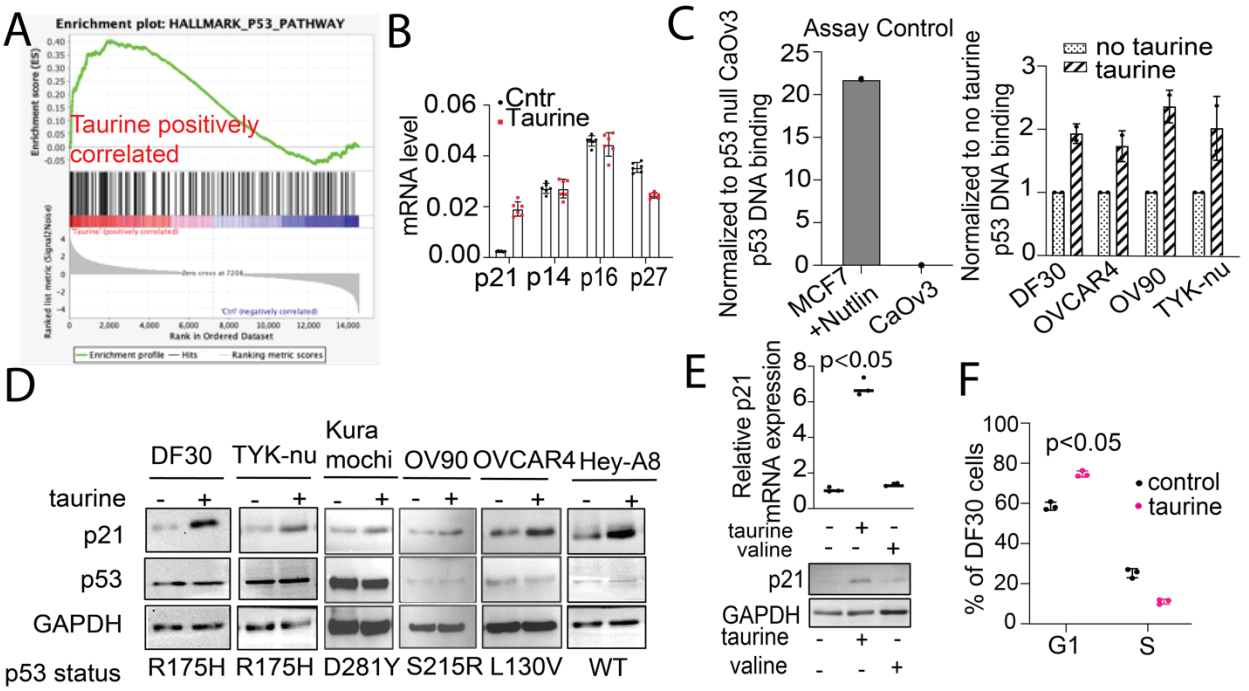

Figure 5. *(A)* Differential transcriptomic analysis of *TP53* gene pathway in DF30 cell monolayers grown under normal conditions or in media supplemented with taurine. *(B)* Quantification of mRNA expression levels of cyclin-dependent kinase inhibitors in DF30 cell monolayers cultured in the absence or presence of taurine. *(C)* ELISA based p53-DNA binding assay. Each dot represents one biological replicate. *(D)* Western blot analysis of p21, p53, and GAPDH protein expression in various OC lines expressing mutant or wild-type p53. *(E)* p21 mRNA quantification and western blot analysis of p21 and GAPDH expression in DF30 cells cultured in the absence or presence of taurine or valine. *(F)* Flow-cytometry and PI-based cell-cycle analysis of DF30 cell monolayers cultured in the absence or presence of taurine. Each dot represents one biological replicate. An unpaired, two-tailed t-test was used to determine statistical differences between the means.

Fig. 5B). Moreover, taurine supplementation did not activate CDKN2A (p14 or p16), and CDKN1B (p27) transcription (Fig. 5B), further supporting the role of *TP53*-mediated cell-cycle regulatory pathways. Next, we wondered whether taurine activation of p21 mRNA expression correlates with increased mutant or wild-type p53 binding to DNA. We used commercially available p53-DNA binding assays Kit (Cayman, #600020), and found that, in various OC cell lines, taurine increased mutant or WT p53 protein interaction with DNA (Fig. 5C). As a negative control, we used a nuclear extract of CaOv3 cells which do not express p53, and a positive control was represented by treatment of MCF7 (WT p53) with Nutlin (p53 protein stabilizer) (Fig. 5C). Our results raised the possibility that taurine increases p21 promoter activity leading to p21 protein expression. To

extend these studies to living cells, we have engineered, based on el-Deiry's p21 reporter[54], a live p21-mCherry promoter (containing a p53 response element) nuclear biosensor, that upon activation, produces fluorescence in living cells (S. Fig. 2A). As a control we used nuclear CSII-mCherry with EF1a promoter that does not contain p53 response elements (Addgene #125262). We found that in OC cells expressing WT or mutant p53, taurine supplementation increased p21 but not EF1a promoter activity, as measured by flow cytometry (S. Fig. 2B). Consistent with these data, western blot analysis revealed taurine-induced p21 upregulation in a panel of OC cell lines expressing various mutant p53 and WT p53 proteins (Fig. 5D). In addition to OC cell lines that express mutant p53, taurine supplementation of FNE or FNE-m-p53 cells, but not FNE cells expressing shRNA-targeting p53 mRNA, led to the activation of p21 transcription (S. Fig. 2C). and protein expression (S. Fig 2D). Supplementation of DF30 cultures with 160 mM of valine did not induce p21 activation (Fig. 5E), further supporting taurine specificity in activation of the p53 pathway. Moreover, taurine failed to stimulate p21 in CaOv3 OC cells that do not express p53 protein (S. Fig. 2E). p21 can arrest the cell cycle in the Gap1 (G1) phase[55], so we hypothesized that taurine-supplementation arrests cells in the G1. To examine the cell-cycle progression, we used flow-cytometry-based measurements of DNA content. Our experiments, using multiple cell lines, revealed that taurine significantly increased the percentage of cells residing in the G1 phase, and decreased the percentage of cells in the S phase (Fig. 5F and S. Fig. 2F). Taken together, these data support the involvement of WT p53 protein and various mutant p53 proteins in taurine-mediated activation of p21.

Taurine activates TIGAR and suppresses metabolism independently of p53.

Taurine supplementation of CaOv3 cell cultures did not activate p21 (S. Fig. 2E) but decreased cell proliferation by ~30% (Fig. 6A), indicating that taurine can activate tumor suppression independent of p53 and p21 expression. Our RNA-seq experiment revealed that taurine supplementation altered gene transcripts involved in glycolysis and pyruvate oxidation (Fig. 6B),

the biochemical pathways that, independent of p53 expression, can generate energy to

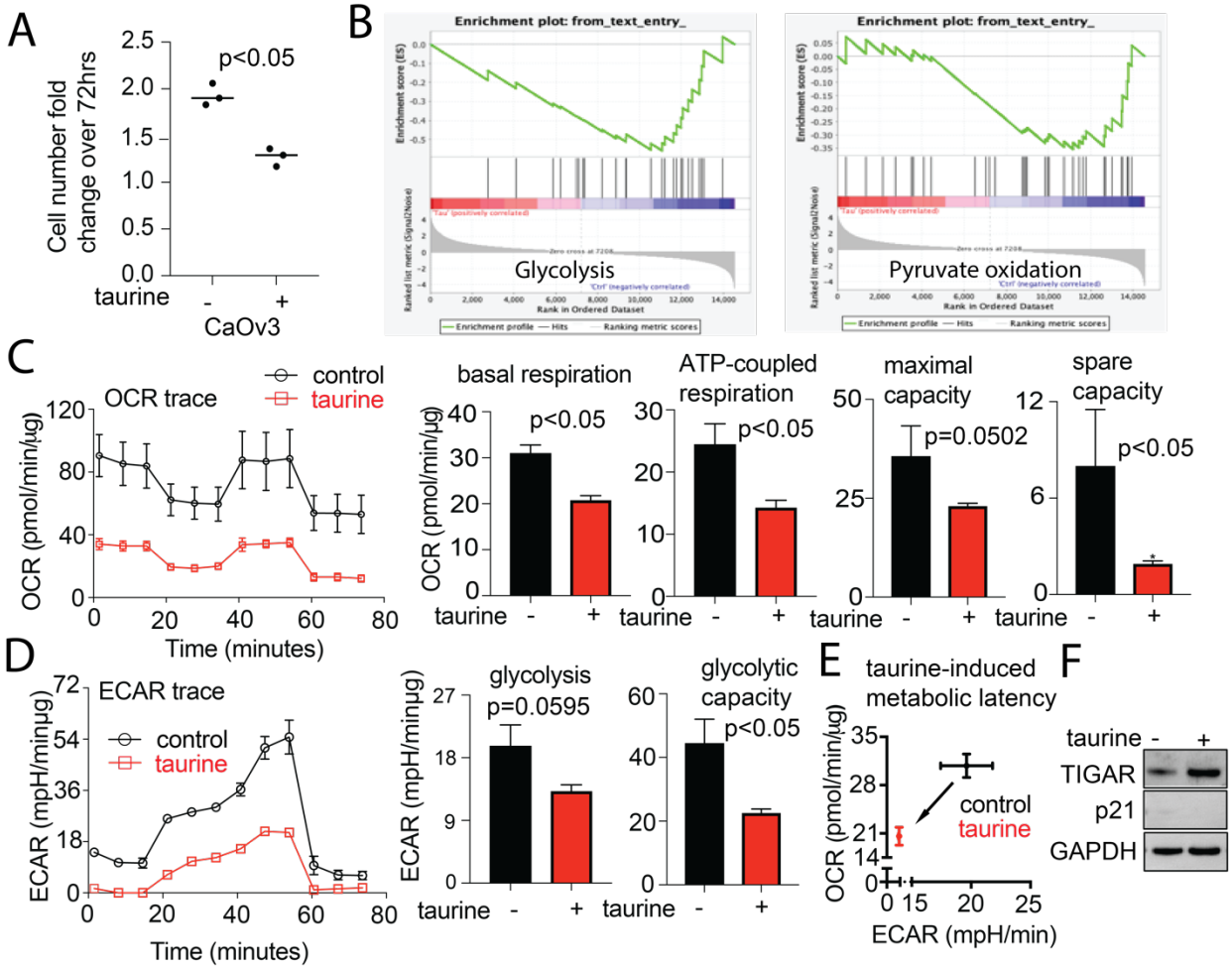

Figure 6. *(A)* Quantification of cell proliferation, based on automatic counting, in CaOv3 cell monolayers, supplemented with growth media or growth media containing taurine. Each dot represents one biological replicate. *(B)* Enrichment analysis of transcripts corresponding to genes implicated in the regulation of glycolysis and pyruvate oxidation. *(C)* Mitochondrial capacity analysis in CaOv3 monolayers supplemented with media or media containing taurine. The line graph shows representative OCR over time. Bar graphs show average values with standard deviations (maximal whiskers) across three experiments. *(D)* Analysis of ECAR over time representing glycolysis and glycolytic capacity. Bar graphs show average values with standard deviations (maximal whiskers) across three experiments. An unpaired, two-tailed t-test was used to determine statistical differences between the means. *(E)* Graph representing a taurine-induced decrease in OCR and ECAR rates in CaOv3 cells. (F) Western blot analysis of TIGAR, p21, and GAPDH expression in CaOv3 cell monolayers.

support cell proliferation[56]. To address the possible hampering of metabolism by taurine, we first determined mitochondrial respiration and their capacity in CaOv3 cell monolayers supplemented with taurine. We found that taurine significantly suppressed mitochondrial function including

oxygen consumption rate (OCR) and the maximal respiratory capacity (Fig. 6C). We next examined whether taurine also inhibits extracellular acidification rates (ECAR), as a proxy of glycolytic activity. ECAR analysis revealed that taurine suppressed glycolysis and glycolytic capacity (rate of conversion of glucose to pyruvate/lactate) in CaOv3 cells (Fig. 6D). Our data provide evidence that supplementing taurine into CaOv3 cell monolayer cultures causes a shift from metabolically active towards a latent metabolic state (Fig. 6E), which is consistent with the suppression of cell proliferation and activation of a negative glycolysis-regulatory phosphatase the TP53-Inducible Glycolysis and Apoptosis Regulator (TIGAR) (Fig. 6F). Taken together, our data indicate that taurine induces growth suppression of OC cells through p53-dependent (p21) and independent (TIGAR) mechanisms including activation of the cell-cycle and metabolic inhibitory pathways.

Expression of p21 or TIGAR mimics taurine-induced inhibition of OC cell proliferation.

To determine whether activation of tumor suppression pathways, which were evoked by taurine treatment, is sufficient to suppress OC cell growth, we used lentiviral transduction to express a plasmid containing doxycycline-regulated p21 in DF30 and Hey-A8 cells (Fig. 8A). As expected, we observed that in both cell lines, elevation of p21 expression was sufficient to decrease proliferation of cells grown as 2D monolayers (Fig. 8A). Furthermore, expression of p21 suppressed the formation of Hey-A8 outgrowths under reconstituted basement-membrane conditions (Fig. 8B), further supporting that role of p21 expression in the inhibition of OC growth. We next set to determine whether overexpression of TIGAR in CaOv3 cells is sufficient to suppress cell proliferation. We discovered that doxycycline-regulated TIGAR expression decreased CaOv3 cell proliferation by ~22% (Fig. 8C). These results support the idea that either p21 or TIGAR is sufficient to restrict growth of OC cells, and taurine's OC growth suppression mechanisms could involve activation of p21-dependent cell-cycle control and/or TIGAR regulation of metabolism.

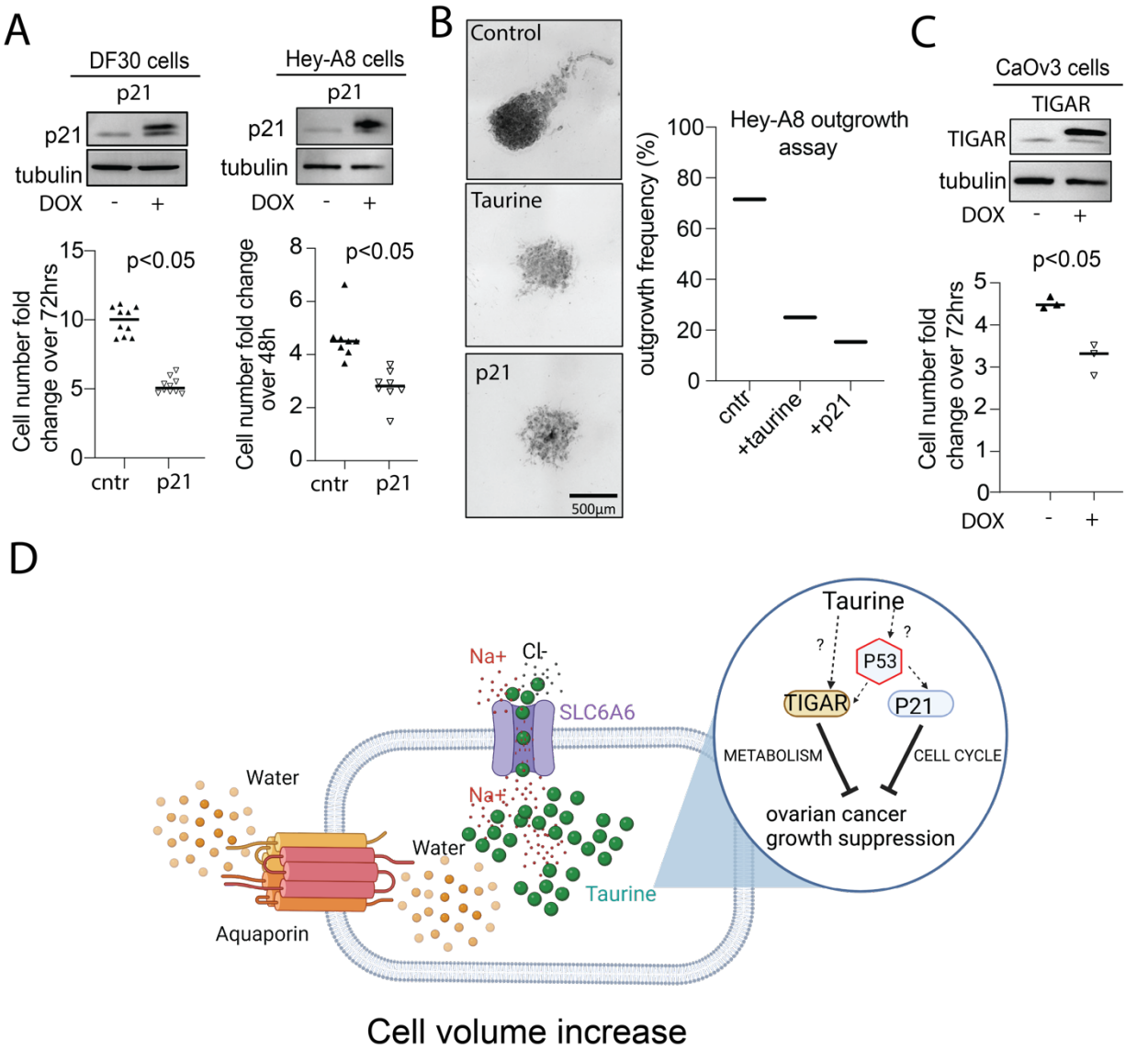

Figure 7. *(A)* Western blot analysis of p21 and tubulin expression in DF30 and Hey-A8 cells expressing plasmid containing doxycycline-regulated p21. Dot plots represent time-lapse assisted cell proliferation measurements based on GFP-positive cell tracking. Each dot corresponds to one region of interest that contained 20-50 cells. An unpaired, two-tailed t-test was used to determine statistical differences between the means. *(B)* Representative, same-scaled, bright-field images of various Hey-A8 cell assemblies forming outgrowths. Graph represents quantification of frequency of outgrowth formation by control Hey-A8 cells or Hey-A8 cells treated with taurine or overexpressing p21. *(C)* Western blot analysis of TIGAR and GAPDH expression in CaOv3 cells expressing doxycycline-regulated TIGAR. Dot plot representing quantification of CaOv3 cell proliferation. Each dot represents one replicate count. *(D)* Graphical representation of taurine-mediated suppression of OC growth.

In summary, we provide evidence that the taurine can activate tumor suppressor pathways and inhibit cancer cell proliferation in various OC cells (including chemotherapy-resistant) carrying WT or *TP53* gene mutations. Taurine's tumor suppressive activities involved cell volume increase, p53 biding to DNA, p53-dependent activation of p21 promoter, increased expression of p21 protein, G1 arrest, activation of TIGAR, and inhibition of glycolysis and mitochondrial function.

DISCUSSION

These studies provide potentially new insights into the mechanisms of OC growth suppression by taurine, a sulfonic non-proteogenic amino acid and a common dietary supplement. The biochemical examination of human FNE cells, patient-derived cells, OC cell cultures, and patient ascites made it possible to identify the SLC6A6 and taurine as molecular components of OC and its TM. The data presented here are consistent with the model that exogenous taurine supplementation, that exceeds taurine levels found in OC TMs, induces SLC6A6-dependent taurine intracellular accumulation which correlates with OC cell area and cell volume increase, suppression of OC cell metabolism and growth (Fig. 7D). Our experiments revealed that taurine supplementation activates inhibitors of the cell cycle and metabolism, including p21 and TIGAR, and ectopic expression of p21 or TIGAR in OC cell lines was sufficient to suppress OC cell proliferation.

Ovarian tumors that arise in the fallopian tube, can lose cell-cycle regulation, in part, through the inactivation of the p53/p21 pathway[57]. Low levels of nuclear p21 in ovarian tumors correlate with tumor cell proliferation and reduced progression-free interval for patients[8-11]. Platinum-based chemotherapy, a standard approach to treat OC[58], can activate p21 and arrest the cell cycle in OC cells[59,60]; however, due to overt cell toxicities and emerging chemotherapy resistance, the treatment is temporary, and, in most cases, surviving tumor cells regain the ability to proliferate and cause disease progression. In this study, we provide evidence that supplementation of OC cell cultures with the dietary supplement taurine activates cell-cycle control without causing cytotoxicity in OC cells expressing wild-type p53 protein or various full-

length mutant p53 proteins. In these cell lines, we observed that taurine-mediated suppression of proliferation correlated with p53 binding to its DNA responsive elements, activation of the p21 promoter, and p21 protein expression. Overexpression of p21 in OC cells mimicked taurine-induced inhibition of proliferation, further supporting the idea that taurine could potentially provide a strategy to inhibit OC cell proliferation through the activation of a major cell-cycle inhibitory pathway. Our data are consistent with recent *in silico* and cell-free biochemical studies[61] demonstrating that taurine can directly bind cyclin-dependent kinase 6 (CDK6). This interaction appears to inhibit CDK6 activity in solution, supporting the possibility that intracellular taurine accumulation could directly suppress CDK6/Cyclin D activity and arrest the cell cycle in G1 (demonstrated by our data). Thus, taurine-mediated inhibition of carcinoma cell proliferation could potentially involve inhibition of CDK6 and, through p53, activation of p21 leading to G1 arrest.

Some *TP53* mutations result in the loss of p53 protein expression preventing the induction of p53-mediated p21 and cell-cycle suppression. We discovered that taurine supplementation could suppress OC cell proliferation in the absence of p53 protein and p21 activation, implicating that taurine activates distinct tumor suppression pathways. Our RNA-seq analysis revealed that, in addition to activation of p21, taurine inhibited energy generation through suppression of glycolysis and mitochondrial oxidative phosphorylation. The literature provides evidence that depletion of taurine results in a significant increase in glucose utilization[62], and taurine supplementation decreases glycolysis[63,64]. These and our studies are consistent with the idea that, in addition to direct regulation of the cell cycle, prolonged exposure to taurine could inhibit tumor growth by interfering with energy production to shift tumor cells into a growth-suppressed state. Consistently, taurine-induced activation of the negative regulator of glycolysis, TIGAR, and ectopic expression of TIGAR was sufficient to decrease OC proliferation independently of taurine. TIGAR is a phosphatase that inactivates phosphofructokinase-1 (PFK1) a key glycolytic enzyme involved in glycolytic flux[65]. TIGAR can be regulated by p53-dependent[65] and independent[66] pathways, and we provide evidence that taurine promotes TIGAR in OC cells that lack p53 protein

expression. How taurine activates TIGAR expression in the absence of p53 is not clear. One of the possibilities could be that taurine activates TIGAR through the regulation of Cyclic AMP-responsive Element Binding protein (CREB) expression or phosphorylation[67,68].

Taurine is an osmolyte that can regulate cell volume and cell size. Depletion of intracellular taurine through β-alanine supplementation[49] or taurine transporter knockout results in atrophic hearts and reduced myocyte size[69]. In OC cells, we found that a 20-fold rise in intracellular taurine levels correlated with increases in cell size and cell volume. These changes were associated with the induction of cell-cycle arrest, decreased metabolism, and suppression of OC cell proliferation. Taurine plasma levels decline during aging[26], a process associated with decreased p53 function[70], and increased cancer incidence[71]. Interestingly, taurine supplementation activates anti-aging mechanisms in mice[26], and in this report we provide evidence for taurine-mediated restoration of p53 function in cultured OC cells carrying mutant or wild-type p53. Our data support the model that increasing taurine levels within TMs might suppress tumor growth through mechanisms associated with cell size and cell volume regulation. Further investigation of these mechanisms might inform novel strategies to suppress OC cell growth. Because our studies are limited to cell culture experiments, in which a high concentration of taurine is used, it remains to be determined whether a high-dose taurine diet can suppress OC growth *in vivo* or in patients.

Supplementary figures

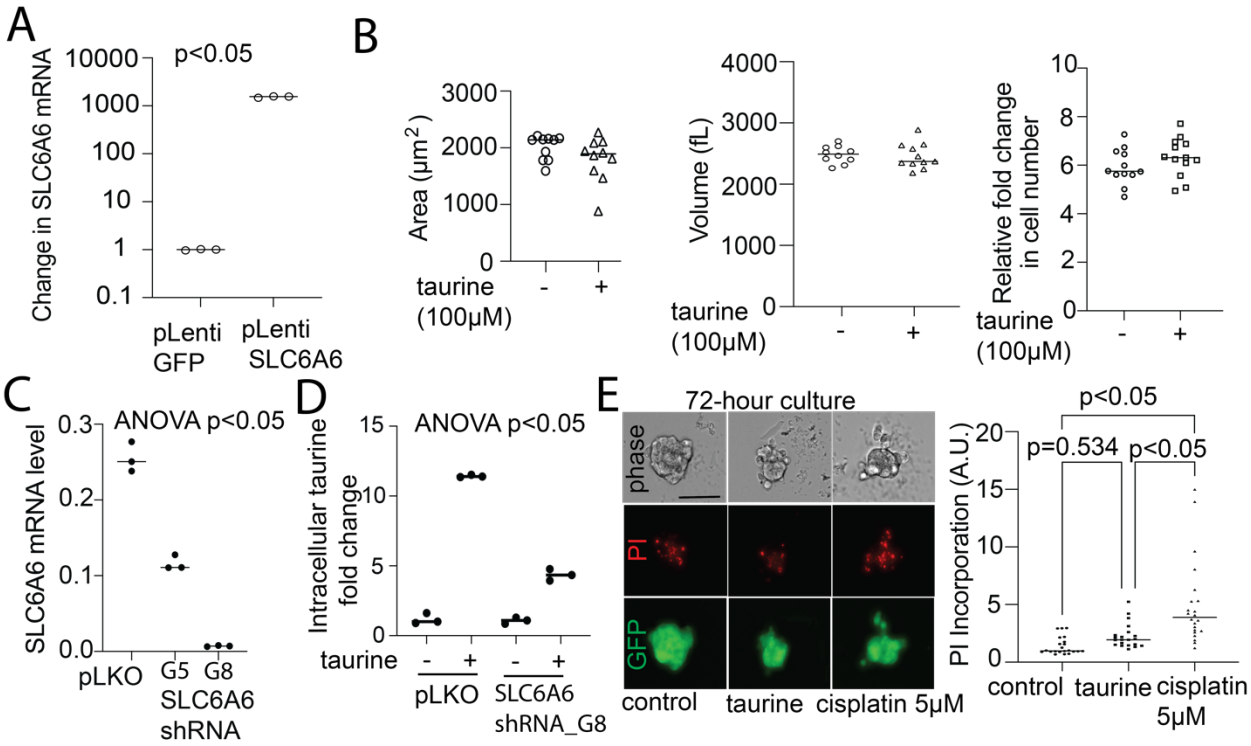

Supplementary Figure 1. *(A)* Quantification of SLC6A6 mRNA in HEK293 cells expressing a control plasmid or a plasmid containing SLC6A6. An unpaired, two-sided t-test was used to determine the difference between the means. *(B)* Quantification of DF30 cell adhesion area, cell volume, and cell proliferation in the absence or presence of 100 μM of taurine supplementation. Each dot represents one ROI containing 25-100 cells. *(C)* Quantification of SLC6A6 mRNA in control or DF30 cells expressing plasmid containing shRNA sequences G5 and G8 targeting SLC6A6 mRNA. Each dot represents one replicate. *(D)* Quantification of intracellular levels of taurine in DF30 cells expressing a control or plasmid containing SLC6A6 shRNA G8 cultured in the absence or presence of taurine. Each dot represents one replicate. *(E)* Equal magnification fluorescent images of suspended DF30 cell spheroids (phase) expressing GFP (green) and treated with propidium iodide (red) and cultured in the absence or presence of taurine or cisplatin. The scale bar is 200 μm. Quantification of DF30 spheroid viability based on PI incorporation. Each dot represents one spheroid. One-way ANOVA followed by the post-hoc Sidak correction was used to determine the difference between the means (horizontal lines).

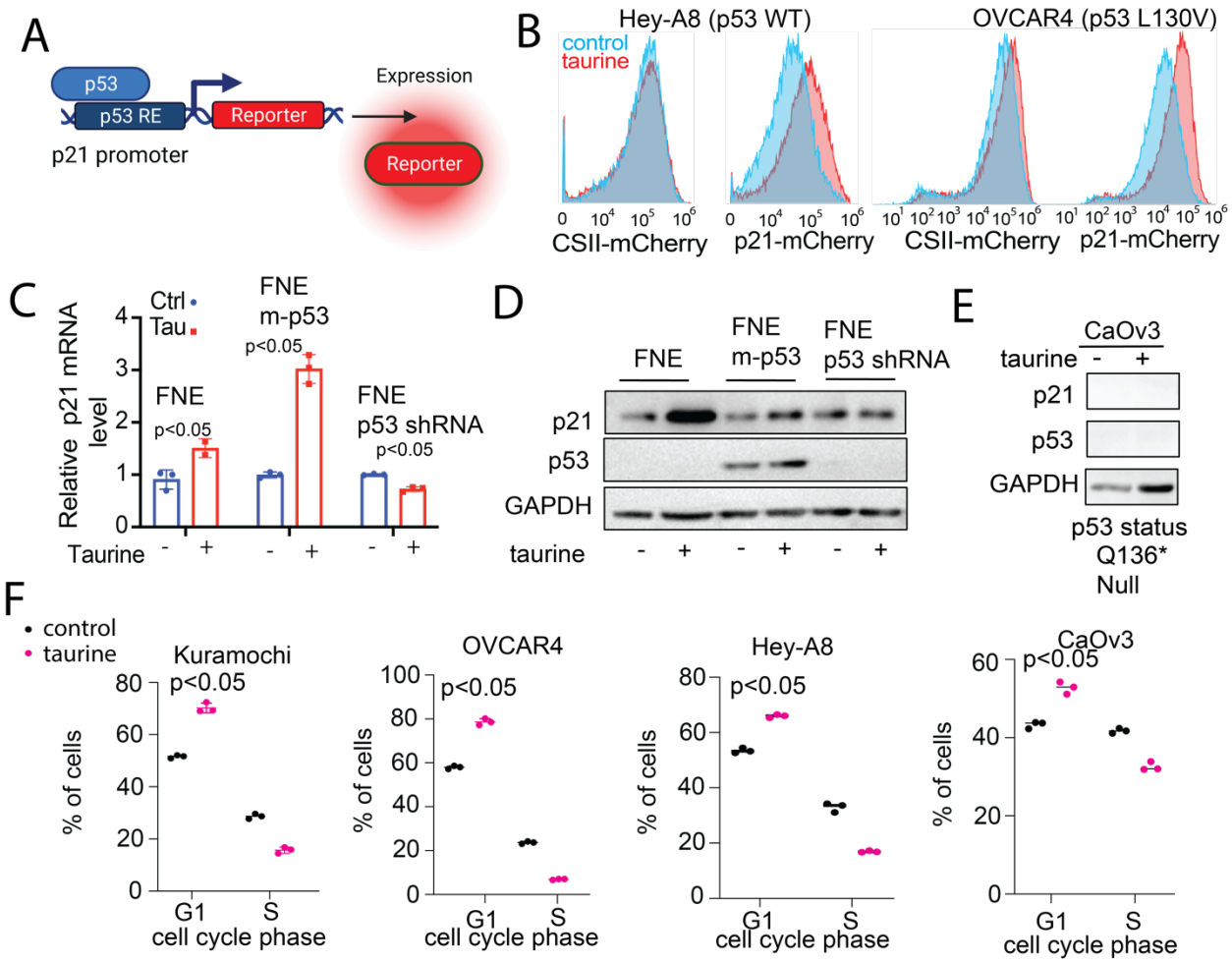

Supplementary Figure 2. *(A)* Schematic representation of p21 promoter biosensor. *(B)* Histogram representation of flow cytometry-based analysis of taurine-induced p21 promoter activation. *(C)* Measurment of p21 mRNA in various syngenic FNE cell lines. Each dot represents one biological replicate. Unpaired, two-sided t-tests were used to determine difference. *(D)* Western blot anlysis of p21, p53, GAPDH in syngenic FNE cell lines. *(E)* Western blot analysis of p21 and p53 in CaOv3 cell line. *(F)* Flow-cytometry and PI -based cell cycle anlysis of cell monolayers cultured in the absance or presence of taurine. Each dot represents one replicate. An unpaired, two-tailed t-test was used to determine statistical differences between the means.

Experimental procedures

Cell culture

DF30 (kind gift from Dr. Ronny Drapkin, University of Pennsylvania) and FNE cells (kind gift from Dr. Tan Ince, Weill Cornell Medicine, New York) were cultured in a 1:1 ratio of DMEM/F12 (HiMedia), and Medium 199 (HiMedia), 2% heat-inactivated Fetal Bovine Serum (HI-FBS; Sigma-

Aldrich), 1% *v/v* penicillin-Streptomycin (VWR), 0.5 ng/mL of beta-estradiol (US Biological), 0.2 pg/mL of triiodothyronine (Sigma-Aldrich), 0.025 μg/mL all-trans retinoic acid (Beantown Chemical), 14 μg/mL of insulin (Sigma-Aldrich), 0.5 ng/mL of EGF (Peprotech), 0.5 μg/mL hydrocortisone (Sigma-Aldrich), and 25 ng/mL of cholera toxin (Calbiochem). Kuramochi, OVCAR4, and OV90 (kind gift from Dr. Denise Connolly, Fox Chase Cancer Center) and HEK293T cells (Thermo Fisher) were cultured in DMEM/F12 supplemented with 10% HI-FBS and 1% v/v penicillin-Streptomycin. CaOv3 (ATCC), HEY-A8 (kind gift from Dr. Sumegha Mitra's laboratory, University of Indiana), and TYK-nu (kind gift from Dr. Joan Brugge's laboratory, Harvard Medical School) cells were cultured in a 1:1 ratio of MCDB 105 (Sigma-Aldrich) and Medium 199 supplemented with 5% HI-FBS and 1% v/v penicillin-Streptomycin. OV81-CP, OV81-CP40 and OV231 , OV231-CP30 were cultured in DMEM/F12 supplemented with 10% HI-FBS and 1% v/v penicillin-Streptomycin. All cell lines were cultured in a humidified incubator at 37°C and with 5% carbon dioxide. Cell cultures were tested for the presence of mycoplasma every 3-6 months using the Uphoff and Drexler detection method[72]. Taurine (TCI Chemicals) was dissolved directly into complete cell culture media at a concentration of 40 mg/mL and passed through a 0.22 micron filter before treatment.

Labeling and enrichment of cell surface proteins and mass spectrometry experiment

To enrich cell surface proteins for mass spectrometry analysis, we followed the protocol from Weekes *et al*.[73] Briefly, cells were grown in suspension for three days. On the third day of suspension culture, cells were placed on ice and subjected to treatment with oxidation/biotinylation mix containing ice-cold PBS solution of 1 mM sodium-meta periodate, 100 mM aminooxy-biotin (Biotium, INC.) and 10 mM Aniline (Sigma). The oxidation/biotinylation reaction was quenched with 1 mM glycerol after 30 minutes. Cells were washed twice with ice-cold PBS pH 7.4. Cells were lysed in lysis buffer containing 1% Triton X-100 (high purity

ThermoFisher), 150 mM NaCl, 1X protease inhibitors (Roche), 5 mM iodoacetamide (Sigma), 0.1 mg/ml PMSF and 10 mM Tris-HCL pH 7.6. Cell lysates were spun twice at 16,000 x *g*, and supernatants were used to enrich for biotinylated proteins by incubating for two hours at 4°C with streptavidin agarose beads. After the enrichment step, beads were washed extensively with lysis buffer followed by PBS/0.5% (*w/v*) SDS wash. Beads were incubated for 20 minutes with PBS/0.5% SDS containing 100 mM DTT. Further washing was performed with UC buffer containing 6M urea, 100 mM Tris-HCL pH 8.5, followed by 20 minutes, at room temperature, an alkylation reaction in the additional presence of 50 mM iodoacetamide. Beads were washed in UC buffer, 5M NaCl, 100 mM Na_2CO_3, PBS then water, resuspended in 400 μL 50 mM NH_4HCO_3 containing 5 μg modified sequencing grade trypsin (Promega), then transferred to a protein LoBind tube (Eppendorf) for overnight digestion. The next day, tryptic digests were eluted in Pierce^{TM} Snap-Cap spin columns. Eluted peptides labeling was performed as described before[47]. Briefly, desalted peptides were dissolved in 100 mM HEPES pH 8.5. 100% of each sample was labeled with TMT. TMT reagents (0.8 mg) were dissolved in 40 μM anhydrous acetonitrile and 2.5 μL were added to a peptide final acetonitrile concentration of 30% (*v/v*). Mass spectrometry data were acquired using an Orbitrap Elite mass spectrometer coupled with Proxenon EASY-nLC 1000 LC pump (Thermo Fisher). Mass spectra were processed using a Sequest-based in-house software pipeline. MS spectra were converted to mzXML by ReAdW.exe. Database was constructed from the human Uniprot database. Clustered heatmaps of the first 110 significant relative protein reads for taurine treated and control samples were generated with R function heatmap.2 from the gplots package, which generates highly customizable heatmaps. The heatmap was extracted based on the mass spectrometry read values on a logarithmic scale. Hierarchical clustering of this data was performed using the function hclust available by Cluster package (version 2.1.4).

Patients Ascites

From 2021 to 2022, we enrolled in the study Caucasian patients with histologically confirmed high-grade serous ovarian cancer and ascites in the Department of Gynecologic Oncology, Poznan University of Medical Sciences. Ovarian tumors were staged according to FIGO (International Federation of Gynecology and Obstetrics) system. Ascites fluid samples were collected from patients (i) at laparoscopy before starting the neoadjuvant chemotherapy and (ii) by paracentesis in women with recurrent disease. Ascites fluid (10 mL) was centrifuged within 2 hours after collection in a falcon tube at 1,100 × *g* for 10 minutes at room temperature to separate a cell pellet. The supernatant was stored in -80°C and analyzed collectively after completion of the study. All patients provided a signed informed consent, approved by the Ethics Review Board of Poznań University of Medical Sciences (Consent No 737/17). All procedures performed in studies involving human participants were in accordance with the ethical standards of the institutional and national research committee and with the 1964 Helsinki declaration and its later amendments or comparable ethical standards.

Mass-spectrometry-based quantification of taurine levels in ascites and cell lysates

The panel of amino acids was quantified based on aTRAQ kit for amino acid analysis (SCIEX, Framingham, MA, USA) and liquid chromatography coupled to a triple quadrupole tandem mass spectrometry technique. The samples (ascites or cell lysates) were thawed at room temperature, and 40 µL of a matrix was transferred to a 0.5 mL Eppendorf tube. Then, 10 µL of sulfosalicylic acid was added to precipitate the proteins, and the vial contents were mixed and centrifuged. Subsequently, 10 µL of supernatant was transferred to a clean tube, and 40 µL of borate buffer was added, mixed, and centrifuged. In the next step, the 10 µl of obtained mixture was transferred to a clean tube and mixed with 5 µL of amino labeling reagent (aTRAQ Reagent Δ8®). After centrifugation, samples were incubated for 30 minutes at room temperature. The incubation was followed by the addition of 5 µL of hydroxylamine solution, mixing and centrifugation. Then the

samples were incubated for 15 minutes at room temperature. In the next step, 32 µL of freshly prepared internal standards solution was added, mixed up, and centrifuged. The contents of the tubes were concentrated (temperature 50°C for about 15 minutes) to a volume of about 20 µL using a vacuum concentrator (miVac Duo, Genevac, Stone Ridge, NY, USA). In the last step, 20 µL of ultrapure water was added to each vial and mixed. The contents of the tubes were transferred to amber-glass autosampler vials with inserts. Samples were analyzed in random order by chromatographic separation followed by tandem mass spectrometry detection LC-MS/MS.

The analytes were separated on a Sciex C18 column (4.6 mm × 150 mm, 5 µm) maintained at 50 °C using a 1260 Infinity HPLC instrument (Agilent Technologies, Santa Clara, CA, USA). A gradient flow of the mobile phase was applied. The mobile phase consisted of 0.1% formic acid (FA) and 0.01% heptafluorobutyric acid (HFBA) in water—phase A, and 0.1% FA and 0.01% HFBA in methanol—phase B, maintained at a flow rate 800 µL/min. Total runtime was 18 minutes per sample, with injection volume equal to 2µL. Detection and quantitation of analytes were performed by means of a quadrupole tandem mass spectrometer with an electrospray ionization (ESI) TurboV ion source operated in positive ion mode. All results were generated in a scheduled multiple reaction monitoring mode. Raw data from amino acids assays was acquired and analyzed using the Analyst software version 1.6.3 (Sciex, Framingham, MA, USA). The method validation and sample preparation were described in detail before [51]

Quantification of taurine levels in cell lysates using a commercial kit

To determine the intracellular taurine concentration, a Taurine Assay Kit (Cell Biolabs, Inc.) was used. Cells were treated with taurine for the indicated amount of time, washed three times with PBS, lysed in ice-cold RIPA buffer to extract intracellular contents, and protein content was determined using BCA Assay. Then, 25 µg of protein were loaded into a 96-well plate in triplicate for each sample. Taurine concentration was determined using the Taurine Assay Kit following the

manufacturer's instructions, and absorbance values were read at 405 nm using a SpectraMax i3x Multi-Mode Microplate Reader (Molecular Devices). Absorbance values were then background subtracted and normalized to the average absorbance value of the control group. Values were reported as fold change in intracellular taurine concentration.

Organoid derivation and culture

Organoids were derived from primary tissue tumor samples of patients with ovarian cancer as described by Kopper et al.[74]. Briefly, fresh tumor resections were cut in small pieces. Two to four random pieces were snap frozen and stored in liquid nitrogen for DNA isolation or fixed for histological analysis. The remaining of the tissue was minced, digested with 0.7 mg/ml collagenase (Sigma C9407) in the presence of 10 μM ROCK inhibitor (Y-27632 dihydrochloride, Abmole) at 37°C for 25-50 minutes and strained over a 100 μm filter. The digested tissue suspension was centrifuged at 300 x g for 5 minutes. Visible red pellets were lysed with red blood lysis buffer (Sigma-Aldrich) for 3 minutes at room temperature and centrifuged at 300 x g for 5 minutes. The dissociated tissue pellet was resuspended in cold Cultrex Reduced Growth Factor BME type 2 (Cultrex BME) (R&D systems) and 25 μl drops per well were plated on pre-warmed 48-well plates. The Cultrex BME/cell suspension droplets were allowed to solidify at 37°C for at least 30 minutes. Solidified droplets with the embedded cells were then overlaid with ovarian tumor organoid medium containing 10 μM ROCK inhibitor (Y-27632 dihydrochloride, Abmole). Medium is composed of: Advanced DMEM/F12 (Gibco) containing GlutaMAX (Gibco), 100 U/mL penicillin, 100 μg/mL streptomycin (Gibco), 10 mM HEPES (Gibco) , 100 μg/mL Primocin® (InvivoGen) , 1x B-27™ supplement (Gibco) , 1.25 mM N-Acetyl-L-cysteine (Sigma-Aldrich), 10 mM Nicotinamide (Sigma-Aldrich), 0.5 μM A83-01 (R&D systems), 0.5 μg/mL Hydrocortisone (Sigma-Aldrich), 10 μM Forskolin (R&D systems), 100 nM β-Estradiol (Sigma-Aldrich), 16.3 μg/mL BPE (Thermo Fisher Scientific) , 10 ng/mL recombinant human FGF-10 (PeproTech), 5

ng/mL recombinant human FGF-7 (PeproTech), 37.5 ng/mL recombinant human Heregulin Beta-1 (PeproTech), 5 ng/mL recombinant human EGF (PeproTech), 0.5 nM WNT Surrogate-Fc fusion protein (ImmunoPrecise), 10% R-Spondin1 condition media and 1% Noggin-Fc fusion protein conditioned medium (ImmunoPrecise). Media was changed every 2-3 days. For established lines, dense cultures containing organoids ranging in size from 100 to 500 μm were passaged every 7-10 days with TrypLE (Life Technologies) containing 10 μM ROCK inhibitor and 10 mg/mL DNase I (Sigma-Aldrich). For Taurine supplementation, 2-Aminoethanesulfonic Acid (TCI chemicals) was freshly added directly to ovarian tumor organoid medium at a 160 mM final concentration, filtered and stored at 4°C . Filtered ovarian tumor organoid medium from the same batch was used as control. For single cell plating, dense organoid cultures were dissociated with TrypLE (Life Technologies) containing 10 μM ROCK inhibitor and 10 mg/mL DNase I (Sigma-Aldrich) for 10 minutes at 37°C followed by mechanical shearing through a 30 G needle, 5x dilution with Advanced DMEM/F12 (Gibco) containing antibiotics, HEPES and GlutaMax as indicated above supplemented with 10 μM ROCK inhibitor and 10 mg/mL DNase I, and centrifugation at 300 x *g* for 5 min. Cell pellets were resuspended in cold Cultrex BME and plated at 200 or 400 cells/μL of BME. Media ± taurine was fully changed every 2-3 days. For organoid collection and plating, 20-50 μm organoids were extracted from the Cultrex BME droplet using cold Cell Recovery Solution containing 10 mg/mL DNase I at 4°C for 30 minutes. The dissolved Cultrex BME containing intact organoids was then collected into 2-3x volume of cold Advanced DMEM/F12 containing 0.1% BSA (Sigma-Aldrich) and 10 mg/mL DNase I and centrifuged at 200-250g for 5 min. The organoid solution is resuspended in cold ovarian tumor organoid medium containing 10% Cultrex BME with or without taurine. The organoid solution is counted prior plating at 500 organoids in 384-well plate format.

Organoid metrics

Brightfield images were acquired and analyzed by a Perkin Elmer Opera Phenix High-Content Screening System and Harmony high-content analysis software (4.9). The area of each organoid was measured with an automated quantification pipeline set up to identify well defined organoid structures in the same focal plane of one single z-plane after selection based on image texture, single structure size and morphology.

Organoid ATP assay

CellTiter-Glo® 3D Assay (Promega) to measure ATP in cells was performed on PDO at the specified experimental endpoint following manufacturer's instructions. Briefly, CellTiter-Glo 3D Reagent was added to each well at 1:1 ratio. Plates were shaken for 25 minutes and luminescence was measured with a ClarioStar Plus reader (BMG).

Cell proliferation analysis

Cell proliferation was determined by two methods: cell counting using fluorescence microscopy or by using an automated cell counter. To assess proliferation by fluorescence microscopy, GFP-expressing cells were seeded in a 12-well plate (CELLTREAT) and incubated overnight. The following day, cells were treated as indicated. Images were captured using an Agilent Biotek LionheartFX automated fluorescence microscope using a 4X objective in the GFP channel immediately after treatment and at the indicated time points. Z-projections were captured for 10-15 regions of interest (ROI) at each time point. Maximum Z-projections of each ROI were generated using Gen5 software (Agilent). To quantify cell number, images were processed with FIJI (FIJI is Just ImageJ) using an in-house macro as follows: images were background subtracted and an automated threshold was applied. Images were then converted to binary and a watershed was applied to separate adjacent cells. The number of particles

(cells) within each image was then measured, and the ratio of cell number at the final time point to the initial time point was reported as the fold change in cell number.

To assess proliferation using an automated cell counter, cells were first seeded into a 12-well plate. The following day, three wells per condition were treated as indicated and another three wells were trypsinized and counted using a Luna II Automated Cell Counter (Logos Biosystems). After 72h of treatment, cells were once again harvested and counted, and cell numbers were normalized to the average value of the initial count and reported as fold change in cell number.

Cell volume and adhesion area quantification

GFP-expressing DF30 or FNE-m-p53 cells were seeded in a 6-well plate and incubated overnight. The following day, cells were treated as indicated and incubated for 72h. Cells were then trypsinized and seeded into a low adhesion 96-well round bottom plates at a density of 100 cells per well. The plate was then centrifuged at 900 rpm for 5 minutes and cell clusters were immediately imaged using an Agilent Biotek Lionheart FX fluorescence microscope. Images were captured using a 10X objective in the GFP and phase contrast channels. To determine cell volume, GFP images were processed in FIJI using an in-house macro. Briefly, images were background subtracted and an automated threshold was applied. Images were then converted to binary and a watershed was applied to separate adjacent cells. The area of each particle (cell) was then measured. From this value, the radius of each cell was determined and volume was estimated from the equation for the volume of a sphere ($V = 4/3\ \pi\ r^3$). Between 15-20 wells were analyzed per condition, and the average volume of a cell per well was reported.

To quantify cell adhesion area, cells were seeded and treated as described for the proliferation assay. At the endpoint, images were captured using an Agilent Biotek LionheartFX microscope with a 10X objective in the GFP and phase contrast channels. Then, as described for the

fluorescence microscopy cell proliferation assay, images were processed in FIJI with an in-house macro and the area of each particle (cell) was reported as cell adhesion area.

Spheroid viability and propidium iodide incorporation assay

The viability of individual spheroids was quantified using a propidium iodide (PI) incorporation assay. PI is a fluorescent dye that intercalates with DNA but is only permeable to the cell membrane of dead or dying cells. The fluorescent intensity of PI was used as an indicator for cell death. Fluorescent intensity in the GFP channel from cells stably expressing GFP was used as an indicator of living cells. GFP-expressing DF30 cells were seeded in an ultra-low adhesion 96 well Nunclon Sphera plate (Thermo Fisher), centrifuged at 900 rpm for 5 minutes, and incubated overnight at 37°C. The following day, spheroids were treated and incubated for the indicated amount of time. PI was then added to media to a concentration of 1 μg/mL and incubated in the dark at 37°C for 30 minutes. Spheroids were then analyzed using an Agilent Biotek LionheartFX fluorescence microscope, and Z-projected images were captured using a 10X objective in the GFP, PI (RFP), and bright field channels. Images were processed using Gen5 software (Agilent) to background subtract and to produce maximum projections of the GFP and PI channels. Then, by utilizing an in-house macro, FIJI (FIJI Is Just ImageJ) was used to assess the integrated fluorescent density within each maximum Z-projection. PI incorporation was calculated as the ratio of integrated density of RFP signal to the integrated density of GFP signal, and all reported values were normalized to the median value of the control group.

Basement-membrane reconstitution and spheroid size quantification

To examine the effects of taurine on basement membrane reconstituted organotypic structures, FNE-m-p53, HEYA8, OV90, OV81-CP and OV231-CP cells were reconstituted in Matrigel® Growth Factor Reduced Basement Membrane Matrix (Corning) as previously described[44]. One hundred cells were seeded per well in a 96-well ultra-low adhesion Nunclon Sphera plate,

centrifuged at 900 rpm for 5 minutes, and incubated overnight. The following day, on ice, Matrigel was added to cell culture media to a concentration of 4% *v/v*. Matrigel solution was then added to each well containing 100 μL of clustered spheroids to a final volume of 200 μL and Matrigel concentration of 2% *v/v*. Z-projections of organotypic structures were captured at the indicated time points using an Agilent Biotek LionheartFX fluorescence microscope using the 4X objective in the bright field and GFP channels. Z-projections were processed into focused stacks using Gen5 software and the area of each structure was measured using FIJI.

RNA sequencing and transcriptomic analysis

RNA extraction was performed by E.Z.N.A.® total RNA kit (Omega Bio-tek) following the manufacturers' protocol. RNA concentration and purity was assessed by NanoDrop 2000 (ThermoFisher). RNA samples were stored at -80°C freezer and subsequently shipped on dry ice to Genewiz (Azenta US, South Plainfield, New Jersey) for RNA sequencing. The RNA sequencing library preparation workflow started with PolyA–based mRNA enrichment, mRNA fragmentation, and random priming followed by first and second strand complementary DNA (cDNA) synthesis. Subsequently, end-repair with 5′ phosphorylation and adenine (dA)–tailing was carried out. Finally, adaptor ligation, PCR enrichment, and Illumina HiSeq 2500 sequencing with two 150–base-pair (bp) runs were performed, and sequence reads were mapped to the reference genome. Bioinformatics analysis workflow started with evaluation of sequence quality and trimming the reads by means of Trimmomatic v.0.36 software to remove possible adapter sequences and nucleotides with poor quality. STAR aligner v.2.5.2b software were applied to map the trimmed reads to the *Homo sapiens* GRCh38 reference genome available on ENSEMBL. To extract gene hit counts, feature Counts from the Subread package v.1.5.2. were used. The hit counts were reported based on the gene ID feature in the annotation file. Only reads that were within the exon regions were considered. The table generated from extracted gene hit counts was used for differential expression analysis. Using DESeq2, gene expression comparison between the taurine

treated and control samples was performed. By using the Wald test, P values and log2 fold changes were calculated. Genes with an adjusted P value (P_{adj}) of less than 0.05 and absolute log2 fold change more than 1 were counted as differentially expressed genes (DEG).

The gene ontology analysis was applied on the statistically significant genes by applying the software GeneSCF v.1.1-p2. The goa_human GO list was implemented to cluster the set of genes based on their biological functions and determine their statistical significance. The gene set enrichment analysis (GSEA) was performed as described earlier (Subramanian et al., 2005) by implementing GSEA_4.2.2. software, against a selected gene sets from Molecular Signatures Database (MSigDB 7.5). GSEA was performed with the ranking metric set to Signal2noise and with number of permutations set to 1000. Plots with false discover rate (FDR) of less than 0.25 were considered as significant.

Flow cytometry

DNA staining (cell cycle analysis) by flow cytometry was performed as follows: cells were harvested by trypsinization, collected by centrifugation, and washed twice with PBS. Cell pellets were then fixed with ice-cold 70% ethanol for at least 30 minutes on ice. Cells were then washed twice with PBS and treated with PBS containing 100 μg/mL RNAse A (Sigma-Aldrich) and 50 μg/mL PI (Molecular Probes) for 30 minutes at room temperature in the dark before analysis. Data acquisition was performed using an Attune NxT Flow Cytometer (ThermoFisher). Data were then analyzed using FlowJo software. To determine cell viability, cell culture supernatant was collected, adherent cells were tryspinized, and were centrifuged at 300 *g* for 5 minutes. Cells were washed twice with PBS containing 2% FBS. Cells were then incubated on ice with PBS containing 2% FBS and 50 μg/mL PI. Data was then acquired by flow cytometry, analyzed using FlowJo, and viability was reported as the percentage of PI-positive cells.

Plasmids

To overexpress p21, pDONR223_CDKN1A_WT (Addgene #82201) was cloned into PCW57.1 (Addgene #41393) using Gateway LR Clonase II (Invitrogen). The PCW57.1 vector contains a tetracycline inducible promoter, and p21 expression was induced by adding 1 μg/mL doxycycline hyclate (Sigma-Adlrich) to cell culture media.

pGenLenti-SLC6A6-FLAG and pGenLenti-TIGAR-FLAG were obtained from GenScript (Piscataway, New Jersey, USA). To generate a doxycycline inducible TIGAR overexpression plasmid, the TIGAR-FLAG sequence from pGenLenti-TIGAR-FLAG was PCR amplified using Q5 High Fidelity DNA Polymerase (New England Biolabs) and was cloned into PCW57.1 at the 5' BSRGI and 3' BAMHI restriction sites using NEBuilder HIFI DNA Master Mix (New England BioLabs).

To generate a p21 reporter plasmid, NEBuilder HiFi DNA Assembly was used to clone a p21 promoter sequence upstream of mCherry-3X-NLS into a lentiviral vector. A sequence containing the 2.4 kbp p21 promoter region was PCR amplified from the pGL2-p21 promoter-Luc (Addgene #33021). The mCherry-3X-NLS sequence was PCR amplified from CSII-prEF1a-mCherry-3X-NLS (Addgene #125262). PCR fragments were assembled into pLenti6.3/V5-DEST-GFP (Addgene #40125) by replacing the CMV promoter and EGFP sequences at the 5' ClaI and 3' SalI restriction sites, respectively. The resulting plasmid (pLenti6.3-p21 promoter-mCherry-3X-NLS) contains the 2.4 kbp p21 promoter upstream of the mCherry-3X-NLS sequence. Plasmid constructs were verified by Next Generation Sequencing.

SLC6A6 shRNA plasmids were obtained from Dharmacon (pLKO.1 vector; TRCN0000038409: TATCACCTCCATATATCCAGG, referred to in this manuscript as G5, and TRCN0000038412: TATACTTGTACTTGTTGTAGC, referred to in this manuscript as G8).

Lentivirus production

To generate lentivirus, packaging plasmids psPAX2 (Addgene #12260) and pMD2.G (Addgene #12259) were mixed with a lentiviral plasmid containing a gene of interest or shRNA and incubated with Lipofectamine 3000 (Invitrogen) in serum free Opti-MEM (Gibco) to generate liposomes containing plasmid DNA. The mixture was then added to HEK293T cells and media was refreshed the following day. Cell culture supernatant containing viral particles was collected 48 hours and 72 hours after transfection. Cell lines were then transduced by adding viral particles to media containing polybrene (Santa Cruz Biotechnology) at a concentration of 10 μg/mL and selected with an appropriate antibiotic 24 to 48 hours after transduction to generate cells stably expressing transgene or shRNA.

RNA Isolation and targeted RT-qPCR analysis

Total RNA was isolated using Quick-RNA Miniprep Kit (Zymo) and reverse transcribed into cDNA using High Capacity cDNA Reverse Transcription Kit (Applied Biosystems) following the manufacturer's instruction. To analyze mRNA expression, 10 ng of cDNA was added to a 10 μL reaction mixture containing Power SYBR Green Master Mix (Applied Biosystems) and primers at a concentration of 330 nM designed to detect the transcript of interest. mRNA levels were quantified using a CFX96 Touch Deep Well Real-Time PCR Detection System (Bio-Rad) and mRNA expression was normalized to a housekeeping gene.

Western Blot Analysis

Cells were washed twice with PBS and lysed in ice-cold RIPA buffer (Cell Signaling Technology) supplemented with a Halt™ Protease Inhibitor Cocktail (ThermoFisher), and cells were collected using a cell scraper. Cell lysates were pelleted at 20,000 x *g* for 20 minutes, supernatant was collected, and protein concentration was determined by BCA Assay (Pierce)

according to the manufacturer's instructions. Lysates were then mixed with 6X sample buffer (375 mM Tris Base, 9% sodium dodecyl sulfate, 50% glycerol, 0.075% bromophenol blue, 9% β-mercaptoethanol), boiled for 10 minutes at 95°C, and then loaded on a polyacrylamide gel and resolved by electrophoresis. Proteins were then transferred to Immobilon membranes (Whatman), blocked with 5% non-fat milk in Tris-buffered saline containing 0.1% *v/v* Tween-20 (TBST) for 30 minutes at room temperature. Membranes were incubated overnight at 4°C in primary antibodies diluted in 5% non-fat milk in TBST. Membranes were then washed three times with TBST and incubated in an HRP-conjugated secondary antibody (1:10,000) for 1 hour at room temperature. Membranes were then washed three times in TBST. Membranes were developed using Immobilon™ Forte enhanced chemiluminescent substrate (Millipore) and visualized using an iBright CL1500 (Thermo Fisher).

Analysis of glycolysis and mitochondrial oxygen consumption rate

Extracellular acidification rate (ECAR) and mitochondrial oxygen consumption rate (OCR) were measured using an XFp Extracellular Flux Analyser (Seahorse Bioscience, North Billerica, MA, USA). The CaOv3 cells were exposed to taurine for 48 hours and then reseeded (8000 cells/well) in taurine-containing media into the wells of an XFp Cell Miniplate. 24 hours later, the cells were analyzed using either XF Cell Mito Stress Test Kit (Seahorse Bioscience) or XFp Glycolysis Stress Test Kit (Seahorse Bioscience) following the manufacturer's instructions.

To measure OCR, cells were washed and incubated with XF Base media (Seahorse Bioscience) supplemented with 1 mM pyruvate, 2 mM glutamine, and 10 mM glucose. After three baseline OCR measurements, 1 μM oligomycin (a mitochondrial ATP synthase inhibitor) was injected followed by sequential injections of 0.5 μM FCCP (a mitochondrial uncoupler), and 0.5 μM Rotenone/Antimycin A (Complex I/Complex III inhibitors of the respiratory chain).

To measure ECAR, cells were washed 3 times with 100 μL of XF Base Media (Seahorse Bioscience) containing 2 mM L-Glutamine. Then the cells were incubated in 180 μL of the same

media for 20 minutes. After three baseline ECAR measurements, cells were subsequently injected with 10 mM glucose, 1 μM oligomycin and 50 mM 2-deoxyglucose (glycolysis inhibitor). After both assays the data obtained were normalized to protein concentrations determined by the bicinchoninic acid (BCA) assay (Pierce, Thermo Fisher Scientific, Waltham, MA, USA).

Wave (Agilent Technology) and GraphPad Prism 8 software were used to analyze and plot the data.

Statistical analysis

Statistical analyses were performed using GraphPad Prism 9.0 (GraphPad Software, San Diego, CA, USA). Statistical significance was determined using an unpaired, two-tailed, parametric t-test with Welch's correction and ordinary one-way ANOVA with Tukey multiple comparisons test, with $p \leq 0.05$ considered statistically significant.

Acknowledgments. We would like to thank Thomas Cattabiani for editorial help with the manuscript preparation. This study was supported by NIH/NCI R21CA256615 (M.I.), an Olipass Corporation grant (M.I.), the Kaleidoscope of Hope Ovarian Cancer Research Foundation (M.I.)., the New York Stem Cell Foundation Research Institute (NYSCF), the NCI R21CA240219 (L.A.M.), Stiftelsen Lars Hiertas Minne FO2021-0082, , Stiftelsen Längmanska kulturfonden BA22-0941, Stiftelsen Sigurd & Elsa Goljes Minne LA2022-0075 (E.K.). Tissue samples were provided by the NCI Cooperative Human Tissue Network (CHTN) RRID SCR_004446. Other investigators may have received specimens from the same tissue specimens.

Competing Interest Statement. No competing interest.

References

1 Bowtell, D. D. *et al.* Rethinking ovarian cancer II: reducing mortality from high-grade serous ovarian cancer. *Nat Rev Cancer* **15**, 668-679, doi:10.1038/nrc4019 (2015).

2 Jimenez-Sanchez, A. *et al.* Heterogeneous Tumor-Immune Microenvironments among Differentially Growing Metastases in an Ovarian Cancer Patient. *Cell* **170**, 927-938 e920, doi:10.1016/j.cell.2017.07.025 (2017).

3 Matulonis, U. A. *et al.* Ovarian cancer. *Nat Rev Dis Primers* **2**, 16061, doi:10.1038/nrdp.2016.61 (2016).

4 Ahmed, A. A. *et al.* Driver mutations in TP53 are ubiquitous in high grade serous carcinoma of the ovary. *J Pathol* **221**, 49-56, doi:10.1002/path.2696 (2010).

5 Cancer Genome Atlas Research, N. Integrated genomic analyses of ovarian carcinoma. *Nature* **474**, 609-615, doi:10.1038/nature10166 (2011).

6 el-Deiry, W. S. *et al.* WAF1/CIP1 is induced in p53-mediated G1 arrest and apoptosis. *Cancer Res* **54**, 1169-1174 (1994).

7 Beckerman, R. & Prives, C. Transcriptional regulation by p53. *Cold Spring Harbor perspectives in biology* **2**, a000935, doi:10.1101/cshperspect.a000935 (2010).

8 Bali, A. *et al.* Cyclin D1, p53, and p21Waf1/Cip1 expression is predictive of poor clinical outcome in serous epithelial ovarian cancer. *Clinical cancer research : an official journal of the American Association for Cancer Research* **10**, 5168-5177, doi:10.1158/1078-0432.CCR-03-0751 (2004).

9 Costa, M. J., Hansen, C. L., Walls, J. E. & Scudder, S. A. Immunohistochemical markers of cell cycle control applied to ovarian and primary peritoneal surface epithelial neoplasms: p21(WAF1/CIP1) predicts survival and good response to platinin-based chemotherapy. *Hum Pathol* **30**, 640-647, doi:10.1016/s0046-8177(99)90088-6 (1999).

10 Werness, B. A., Freedman, A. N., Piver, M. S., Romero-Gutierrez, M. & Petrow, E. Prognostic significance of p53 and p21(waf1/cip1) immunoreactivity in epithelial cancers of the ovary. *Gynecol Oncol* **75**, 413-418, doi:10.1006/gyno.1999.5601 (1999).

11 Terauchi, F. *et al.* Clinical significance of p21(WAF1/CIP1) and p53 expression in serous cystadenocarcinoma of the ovary. *Oncol Rep* **14**, 363-368 (2005).

12 Niculescu, A. B., 3rd *et al.* Effects of p21(Cip1/Waf1) at both the G1/S and the G2/M cell cycle transitions: pRb is a critical determinant in blocking DNA replication and in preventing endoreduplication. *Mol Cell Biol* **18**, 629-643, doi:10.1128/MCB.18.1.629 (1998).

13 Eriksson, M. *et al.* Effect of Mutant p53 Proteins on Glycolysis and Mitochondrial Metabolism. *Mol Cell Biol* **37**, doi:10.1128/MCB.00328-17 (2017).

14 Liu, Y. & Gu, W. The complexity of p53-mediated metabolic regulation in tumor suppression. *Semin Cancer Biol* **85**, 4-32, doi:10.1016/j.semcancer.2021.03.010 (2022).

15 Yu, X. *et al.* Small molecule restoration of wildtype structure and function of mutant p53 using a novel zinc-metallochaperone based mechanism. *Oncotarget* **5**, 8879-8892 (2014).

16 Bykov, V. J. *et al.* Restoration of the tumor suppressor function to mutant p53 by a low-molecular-weight compound. *Nat Med* **8**, 282-288, doi:10.1038/nm0302-282 (2002).

17 Soragni, A. *et al.* A Designed Inhibitor of p53 Aggregation Rescues p53 Tumor Suppression in Ovarian Carcinomas. *Cancer Cell* **29**, 90-103, doi:10.1016/j.ccell.2015.12.002 (2016).

18 Lindemann, A. *et al.* COTI-2, A Novel Thiosemicarbazone Derivative, Exhibits Antitumor Activity in HNSCC through p53-dependent and -independent Mechanisms. *Clinical cancer research : an official journal of the American Association for Cancer Research* **25**, 5650-5662, doi:10.1158/1078-0432.CCR-19-0096 (2019).
19 Mehra, K. K. *et al.* The impact of tissue block sampling on the detection of p53 signatures in fallopian tubes from women with BRCA 1 or 2 mutations (BRCA+) and controls. *Mod Pathol* **24**, 152-156, doi:10.1038/modpathol.2010.171 (2011).
20 Folkins, A. K. *et al.* A candidate precursor to pelvic serous cancer (p53 signature) and its prevalence in ovaries and fallopian tubes from women with BRCA mutations. *Gynecol Oncol* **109**, 168-173, doi:S0090-8258(08)00007-3 [pii]
10.1016/j.ygyno.2008.01.012 (2008).
21 Labidi-Galy, S. I. *et al.* High grade serous ovarian carcinomas originate in the fallopian tube. *Nature communications* **8**, 1093, doi:10.1038/s41467-017-00962-1 (2017).
22 Torre, L. A. *et al.* Ovarian cancer statistics, 2018. *CA Cancer J Clin* **68**, 284-296, doi:10.3322/caac.21456 (2018).
23 de Visser, K. E. & Joyce, J. A. The evolving tumor microenvironment: From cancer initiation to metastatic outgrowth. *Cancer Cell* **41**, 374-403, doi:10.1016/j.ccell.2023.02.016 (2023).
24 Sturman, J. A. Taurine in development. *J Nutr* **118**, 1169-1176, doi:10.1093/jn/118.10.1169 (1988).
25 Stipanuk, M. H. Metabolism of sulfur-containing amino acids. *Annu Rev Nutr* **6**, 179-209, doi:10.1146/annurev.nu.06.070186.001143 (1986).
26 Singh, P. *et al.* Taurine deficiency as a driver of aging. *Science* **380**, eabn9257, doi:10.1126/science.abn9257 (2023).
27 Pasantes-Morales, H. Taurine Homeostasis and Volume Control. *Adv Neurobiol* **16**, 33-53, doi:10.1007/978-3-319-55769-4_3 (2017).
28 Law, R. O. Taurine efflux and cell volume regulation in cerebral cortical slices during chronic hypernatraemia. *Neurosci Lett* **185**, 56-59, doi:10.1016/0304-3940(94)11224-7 (1995).
29 Guizouarn, H., Motais, R., Garcia-Romeu, F. & Borgese, F. Cell volume regulation: the role of taurine loss in maintaining membrane potential and cell pH. *J Physiol* **523 Pt 1**, 147-154, doi:10.1111/j.1469-7793.2000.t01-1-00147.x (2000).
30 Ando, D. *et al.* Function and regulation of taurine transport in Muller cells under osmotic stress. *Neurochem Int* **60**, 597-604, doi:10.1016/j.neuint.2012.02.018 (2012).
31 Hoffmann, E. K. & Lambert, I. H. Amino acid transport and cell volume regulation in Ehrlich ascites tumour cells. *J Physiol* **338**, 613-625, doi:10.1113/jphysiol.1983.sp014692 (1983).
32 Law, R. O. The role of taurine in the regulation of brain cell volume in chronically hyponatraemic rats. *Neurochem Int* **33**, 467-472, doi:10.1016/s0197-0186(98)00051-5 (1998).
33 Jang, H. *et al.* Taurine Directly Binds to Oligomeric Amyloid-beta and Recovers Cognitive Deficits in Alzheimer Model Mice. *Adv Exp Med Biol* **975 Pt 1**, 233-241, doi:10.1007/978-94-024-1079-2_21 (2017).
34 Kim, K. S. *et al.* Taurine ameliorates hyperglycemia and dyslipidemia by reducing insulin resistance and leptin level in Otsuka Long-Evans Tokushima fatty (OLETF) rats with long-term diabetes. *Exp Mol Med* **44**, 665-673, doi:10.3858/emm.2012.44.11.075 (2012).

35 Roman-Garcia, P. *et al.* Vitamin B(1)(2)-dependent taurine synthesis regulates growth and bone mass. *J Clin Invest* **124**, 2988-3002, doi:10.1172/JCI72606 (2014).
36 Terrill, J. R., Pinniger, G. J., Graves, J. A., Grounds, M. D. & Arthur, P. G. Increasing taurine intake and taurine synthesis improves skeletal muscle function in the mdx mouse model for Duchenne muscular dystrophy. *J Physiol* **594**, 3095-3110, doi:10.1113/JP271418 (2016).
37 Young, T. L. & Cepko, C. L. A role for ligand-gated ion channels in rod photoreceptor development. *Neuron* **41**, 867-879, doi:10.1016/s0896-6273(04)00141-2 (2004).
38 Chan, C. Y. *et al.* Direct interaction of taurine with the NMDA glutamate receptor subtype via multiple mechanisms. *Adv Exp Med Biol* **775**, 45-52, doi:10.1007/978-1-4614-6130-2_4 (2013).
39 Mengmeng Yu, Y. W., Zhe Wang, Yanxu Liu, Yang Yu, and Xuejun Gao. Taurine Promotes Milk Synthesis via the GPR87-PI3K-SETD1A Signaling in BMECs. *Journal of Agricultural and Food Chemistry*, 1927-1936, doi:https://doi.org/10.1021/acs.jafc.8b06532 (2019).
40 Rasmussen, R. N., Lagunas, C., Plum, J., Holm, R. & Nielsen, C. U. Interaction of GABA-mimetics with the taurine transporter (TauT, Slc6a6) in hyperosmotic treated Caco-2, LLC-PK1 and rat renal SKPT cells. *Eur J Pharm Sci* **82**, 138-146, doi:10.1016/j.ejps.2015.11.020 (2016).
41 Baliou, S. *et al.* Bromamine T (BAT) Exerts Stronger Anti-Cancer Properties than Taurine (Tau). *Cancers (Basel)* **13**, doi:10.3390/cancers13020182 (2021).
42 Li, H. *et al.* Impact of Taurine on the proliferation and apoptosis of human cervical carcinoma cells and its mechanism. *Chin Med J (Engl)* **132**, 948-956, doi:10.1097/CM9.0000000000000162 (2019).
43 Sorensen, B. H., Thorsteinsdottir, U. A. & Lambert, I. H. Acquired cisplatin resistance in human ovarian A2780 cancer cells correlates with shift in taurine homeostasis and ability to volume regulate. *Am J Physiol Cell Physiol* **307**, C1071-1080, doi:10.1152/ajpcell.00274.2014 (2014).
44 Alshehri, S. *et al.* Extracellular Matrix Modulates Outgrowth Dynamics in Ovarian Cancer. *Adv Biol (Weinh)*, e2200197, doi:10.1002/adbi.202200197 (2022).
45 Iwanicki, M. P. *et al.* Mutant p53 regulates ovarian cancer transformed phenotypes through autocrine matrix deposition. *JCI Insight* **1**, doi:10.1172/jci.insight.86829 (2016).
46 Weekes, M. P. *et al.* Comparative analysis of techniques to purify plasma membrane proteins. *J Biomol Tech* **21**, 108-115 (2010).
47 Weekes, M. P. *et al.* Quantitative temporal viromics: an approach to investigate host-pathogen interaction. *Cell* **157**, 1460-1472, doi:10.1016/j.cell.2014.04.028 (2014).
48 Han, X., Patters, A. B. & Chesney, R. W. Transcriptional repression of taurine transporter gene (TauT) by p53 in renal cells. *J Biol Chem* **277**, 39266-39273, doi:10.1074/jbc.M205939200 (2002).
49 Schaffer, S. W. *et al.* Shape and size changes induced by taurine depletion in neonatal cardiomyocytes. *Amino Acids* **15**, 135-142, doi:10.1007/BF01345286 (1998).
50 Neurohr, G. E. *et al.* Excessive Cell Growth Causes Cytoplasm Dilution And Contributes to Senescence. *Cell* **176**, 1083-1097 e1018, doi:10.1016/j.cell.2019.01.018 (2019).
51 Matysiak, J. *et al.* Effects of a honeybee sting on the serum free amino acid profile in humans. *PLoS One* **9**, e103533, doi:10.1371/journal.pone.0103533 (2014).

52 Belur Nagaraj, A. *et al.* Mitotic Exit Dysfunction through the Deregulation of APC/C Characterizes Cisplatin-Resistant State in Epithelial Ovarian Cancer. *Clin Cancer Res* **24**, 4588-4601, doi:10.1158/1078-0432.CCR-17-2885 (2018).
53 Tuveson, D. & Clevers, H. Cancer modeling meets human organoid technology. *Science* **364**, 952-955, doi:10.1126/science.aaw6985 (2019).
54 el-Deiry, W. S. *et al.* Topological control of p21WAF1/CIP1 expression in normal and neoplastic tissues. *Cancer Res* **55**, 2910-2919 (1995).
55 El-Deiry, W. S. p21(WAF1) Mediates Cell-Cycle Inhibition, Relevant to Cancer Suppression and Therapy. *Cancer Res* **76**, 5189-5191, doi:10.1158/0008-5472.CAN-16-2055 (2016).
56 Wang, P. Y., Zhuang, J. & Hwang, P. M. p53: exercise capacity and metabolism. *Curr Opin Oncol* **24**, 76-82, doi:10.1097/CCO.0b013e32834de1d8 (2012).
57 Piek, J. M. *et al.* Dysplastic changes in prophylactically removed Fallopian tubes of women predisposed to developing ovarian cancer. *J Pathol* **195**, 451-456, doi:10.1002/path.1000 [pii]
10.1002/path.1000 (2001).
58 Cannistra, S. A. Cancer of the ovary. *N. Engl. J. Med.* **351**, 2519-2529 (2004).
59 Ma, Y. *et al.* Mechanism of taurine reducing inflammation and organ injury in sepsis mice. *Cell Immunol* **375**, 104503, doi:10.1016/j.cellimm.2022.104503 (2022).
60 James, N. E. *et al.* Adaptive transcriptomic and immune infiltrate responses in the tumor immune microenvironment following neoadjuvant chemotherapy in high grade serous ovarian cancer reveal novel prognostic associations and activation of pro-tumorigenic pathways. *Front Immunol* **13**, 965331, doi:10.3389/fimmu.2022.965331 (2022).
61 Yousuf, M. *et al.* Inhibiting Cyclin-Dependent Kinase 6 by Taurine: Implications in Anticancer Therapeutics. *ACS Omega* **7**, 25844-25852, doi:10.1021/acsomega.2c03479 (2022).
62 Schaffer, S. W., Shimada-Takaura, K., Jong, C. J., Ito, T. & Takahashi, K. Impaired energy metabolism of the taurine-deficient heart. *Amino Acids* **48**, 549-558, doi:10.1007/s00726-015-2110-2 (2016).
63 Meng, L. *et al.* Taurine Antagonizes Macrophages M1 Polarization by Mitophagy-Glycolysis Switch Blockage via Dragging SAM-PP2Ac Transmethylation. *Front Immunol* **12**, 648913, doi:10.3389/fimmu.2021.648913 (2021).
64 Lan, R. *et al.* Reduction of ROS-HIF1alpha-driven glycolysis by taurine alleviates Streptococcus uberis infection. *Food Funct* **13**, 1774-1784, doi:10.1039/d1fo03909a (2022).
65 Bensaad, K. *et al.* TIGAR, a p53-inducible regulator of glycolysis and apoptosis. *Cell* **126**, 107-120, doi:10.1016/j.cell.2006.05.036 (2006).
66 Lee, P., Hock, A. K., Vousden, K. H. & Cheung, E. C. p53- and p73-independent activation of TIGAR expression in vivo. *Cell Death Dis* **6**, e1842, doi:10.1038/cddis.2015.205 (2015).
67 Liu, J., Liu, Y., Wang, X. F., Chen, H. & Yang, N. Antenatal taurine supplementation improves cerebral neurogenesis in fetal rats with intrauterine growth restriction through the PKA-CREB signal pathway. *Nutr Neurosci* **16**, 282-287, doi:10.1179/1476830513Y.0000000057 (2013).

68 Zou, S. *et al.* CREB, another culprit for TIGAR promoter activity and expression. *Biochemical and biophysical research communications* **439**, 481-486, doi:10.1016/j.bbrc.2013.08.098 (2013).
69 Ito, T. *et al.* Taurine depletion caused by knocking out the taurine transporter gene leads to cardiomyopathy with cardiac atrophy. *J Mol Cell Cardiol* **44**, 927-937, doi:10.1016/j.yjmcc.2008.03.001 (2008).
70 Feng, Z. *et al.* Declining p53 function in the aging process: a possible mechanism for the increased tumor incidence in older populations. *Proc Natl Acad Sci U S A* **104**, 16633-16638, doi:10.1073/pnas.0708043104 (2007).
71 Havas, A., Yin, S. & Adams, P. D. The role of aging in cancer. *Mol Oncol* **16**, 3213-3219, doi:10.1002/1878-0261.13302 (2022).
72 Uphoff, C. C. & Drexler, H. G. Detection of mycoplasma contaminations. *Methods Mol Biol* **290**, 13-23, doi:10.1385/1-59259-838-2:013 (2005).
73 Weekes, M. P. *et al.* Proteomic plasma membrane profiling reveals an essential role for gp96 in the cell surface expression of LDLR family members, including the LDL receptor and LRP6. *J Proteome Res* **11**, 1475-1484, doi:10.1021/pr201135e (2012).
74 Kopper, O. *et al.* An organoid platform for ovarian cancer captures intra- and interpatient heterogeneity. *Nat Med* **25**, 838-849, doi:10.1038/s41591-019-0422-6 (2019).